UNIVERSITY OF
KWAZULU-NATAL

INYUVESI
YAKWAZULU-NATALI

THEORY AND COMPUTER SIMULATION OF HARD-CORE YUKAWA MODELS OF FLUIDS

MSc Dissertation

by

Anele Mkanya

Under the supervision of

Dr. Giuseppe Pellicane

Pietermaritzburg Campus

South Africa

2015

THEORY AND COMPUTER SIMULATION OF HARD-CORE YUKAWA MODELS OF FLUIDS

MSc Dissertation

by

Anele Mkanya

School of Chemistry and Physics

College of Agriculture, Engineering and Science

University of KwaZulu-Natal

Pietermaritzburg,

South Africa

Under the supervision of

Dr. Giuseppe Pellicane

Submitted in fulfillment of the academic requirements for the degree of Master of Science

March 8, 2016

Signed: _____

Date: _____

Preface

The research contained in this thesis was completed by the candidate while based in the Discipline of Physics, School of Chemistry and Physics of the College Of Agriculture, Engineering, and Science, University of Kwazulu-Natal. The research was financially supported by National Institute for Theoretical Physics funds.

The content of this work have not been submitted in any form to another university and, except where the work of other authors is acknowledged in the text, the results reported are due to investigation by the candidate.

Signed: _____

Date: _____

Declaration - Plagiarism

I, <u>Anele Mkanya</u> declare that;

1. The research reported in this thesis, except where otherwise indicated, is my original research.

2. This thesis has not been submitted for any degree or examination at any other university.

3. This thesis does not contain other persons' data, pictures, graphs or other information, unless specifically acknowledged as being sourced from other persons.

4. This thesis does not contain other persons' writing, unless specifically acknowledged as being sourced from other researchers. Where other written sources have been quoted, then:

   a. Their words have been rewritten but the general information attributed to them has been referenced.

   b. Where their exact words have been used, then their writing has been placed in italics and inside quotation marks, and referenced.

5. Where I have used material for which publication followed, I have indicated in detail my role in the work.

6. This thesis is primarily a collection of materials, prepared by my myself, published as journal articles or presented as a poster and oral presentations at conferences. In some cases, additional material has been included;

7. This thesis does not contain, text, graphics or tables copied and pasted from the Internet, unless specifically acknowledged, and the source being detailed in the thesis and in the references section.

Signed: _____

Date: _____

Declaration - Publications

My role in each paper is indicated below each publication.

1. Title : Adsorption of Yukawa fluids on a hard wall

   Authors : Anele Mkanya, Giuseppe Pellicane and Lloyd L. Lee

   Status : Published (*Molecular Physics* (**113**, 1097, (2014)))

   My role in this article was to assist in the adaption of the code to the model being studied, performing the calculations, and helping in editing the subsequent manuscript until it was published.

2. Title : Monte Carlo simulation of symmetric nonadditive hard-core Yukawa mixtures

   Authors : Anele Mkanya, Giuseppe Pellicane and Lloyd L. Lee

   Status : In preparation

   My role in this article was to assist in building the Monte Carlo code, running the computer simulations, and helping in the preparation of the manuscript to be submitted soon.

I have also attended and presented my work in two conferences during the period of my MSc:

1. Centre : NITheP workshop

   Year : 2014

   Type of presentation : seminar

2. Centre : UKZN Research day

   Year : 2015

   Type of presentation : oral

Signed: _____

Date: _____

Abstract

The treatment of long-range Coulomb interactions is still a challenge in computer simulations of fluid systems, even for the primitive model of simple electrolyte solutions. The difficulty is even exacerbated when considering adsorption on a charged wall. For this reason, we focused on charge-screened models of fluids, and we selected the hard core Yukawa fluid (HCYF) model in our study due to its simplicity. We have applied a microscopic, integral equation theory (IET) to the inhomogeneous HCYF and assessed it against Monte Carlo (MC) computer simulations. To this aim, we constructed a bridge functional based on the third-order Ornstein-Zernike (OZ3) equation. For the case of a single-component HCYF in the presence of a hard-wall, the density profiles obtained from the integral equation theory used were found in good agreement with the MC computer simulation ones. The predictions of the new theory were also compared with other microscopic theories reported in the literature: the fundamental measure theory (FMT) and the inhomogeneous integral equation of Lovett-Mou-Buff-Wertheim.

We also considered HCY binary mixtures and we performed extensive MC computer simulations for both additive and nonadditive systems. Our MC data for some selected thermodynamic properties were compared with previously published molecular dynamics (MD) simulations in the scientific literature, and made us conclude that the latter are affected by finite-size effects.

Contents

List of Figures

List of Tables

Acknowledgements

Firstly I would like to thank the Lord for having kept me healthy and strong throughout the period in which this work was carried. Secondly I also would like to offer my special thanks to my supervisor Dr. Giuseppe Pellicane for believing in me and for willing to work with me throughout the duration of this work. He gave me a room to extended my knowledge in the **physics of fluids** field and also to advance my understanding of programming. Without his exceptional encouragement and constant superior guidance which kept me focused, the work that this dissertation entails would not have been completed on time or be of this high quality. The collaboration with Prof. Lloyd L. Lee was fruitful, his participation towards unfolding the information reported in this work is gratefully acknowledged. I am particularly grateful for the assistance given by the technical stuff in making sure that the machines used during the course of this research are of great standard to run the simulations. The friendliness and special help offered by the academic staff and the students of the UKZN physics department in Pietermaritzburg is much appreciated, they all made being on campus much enjoyable. One gets to work more productively if his financial needs are met, with this I would like to acknowledge National Institute for Theoretical Physics (NITheP) for the financial support given to me throughout the two years of my masters degree. My mother Thandeka Tryphina Mkanya is sincerely acknowledged for her motivation, continuous support, encouragement and grooming that she extended towards me since the first day of my journey. This one is for you mom! if it was not for your love, I would not have made it this far. To my family at large, you have been tirelessly behind me from the word go, I extend my appreciation to all of you. My sincere gratitude also goes to Zenande Theresa Msingaphantsi, you have been a good source of strength and you kept me going until the finish line. I love you. Last but not least, I give thanks to my friends for being a family away from home to me in this period of study.

Chapter 1

Introduction

1.1 Rationale for Research

A basic, microscopic model of interaction for fluids is the hard-core Yukawa model (HCYM). This model is one of the most investigated ones in the literature because it includes the two basic ingredients of the pair interaction between two particles in a fluid: the short-range harsh repulsion due to the impenetrability of electronic clouds of atoms, and the long range van der Waals attraction due to induced dipolar interactions. This ability to capture the essential aspects of the microscopic interaction made the HCYM the natural test bench for a number of liquid-state theories [1, 2, 3, 4, 5, 6]. These comparisons to test the reliability of such theories were made by performing computer simulations of the same model, and by looking at a number of properties, including thermodynamic ones [7, 8, 9], and the phase diagram [10, 11, 12, 13, 14]. The HCYM exhibits a genuine liquid-vapour transition, freezing/melting lines, and even iso-structural solid-solid transitions where solid phases with different cubic-symmetry coexist together [15]. The presence of a tunable parameter for the range of the interaction (the Yukawa inverse decay parameter) is an important feature of the model for a number of reasons. One of them is associated to the phase diagram of the model and to the fact that the presence of non-adsorbing polymers in a colloidal solution induces an attractive interaction between the colloidal particles [16]. The spatial range of the attraction between colloids is determined by the radius of gyration of the polymers. Asakura and Oosawa explained (over 50 years ago) that the presence of smaller suspended particles between two surfaces can modify the interaction between the two surfaces [17]. Depending on the range of attraction, the colloids dispersed into the solution can form vapour-like, liquid-like, and even solid-like structures, and there is numerical evidence provided by studying the phase diagram of the HCYM that when the polymer added to the solution has a small radius of gyration, the liquid-like phase disappears [18]. This feature of the phase diagram of the HCYF further enlarged the range of systems for which the model is relevant. In fact, the HCYF is a model that is frequently invoked in the literature in order to

demonstrate short-range interactions between solvated globular proteins [19, 20, 21, 22, 23]. The existence of a small window of negative values of the second virial coefficient of many protein solutions (the so-called crystallization slot [24] that was associated with the presence of a metastable protein-protein demixing region [25]), and the proximity of the critical point to the solubility line of the system (which is achieved within the HCYF with a value of the inverse decay parameter $\lambda\sigma \approx 7$) were observed to favour the process of protein crystallization [25, 26, 27].

These applications of the HCYM are not the only ones to demonstrate that it is not a trivial toy model. In fact, by a proper tuning of its parameters the HCYM can be adapted to mimick more realistic pair potentials, such as the Lennard-Jones one [28]. Tang et al. [29] pointed out that the Lennard-Jones potential can be well approximated by a hard-core repulsion with two-Yukawa tails. With such a model, they were able to predict the thermodynamic and diffusion properties of bovine serum albumin (BSA) in an aqueous electrolyte. The hard-core two-tail Yukawa potential was also adopted to reproduce the phase behaviour of C_{60} fullerene systems [29] and the stability of colloidal dispersions [29]. In principle, the hard-core repulsion with three or more Yukawa tails can be used to approximate any intermolecular potential by taking into account both Van Der Waals and electrostatic interactions. Therefore it is believed that fluid models with multi-Yukawa potentials should be able to mimick real particle interactions of systems quite efficiently [29].

Another important application of the HCYM is the field of charge-stabilized colloids [30] and electrolytes. Charge-stabilized colloidal solutions are made of colloidal particles suspended in a polar solvent in the presence of an electrolyte, so that there are both co- and counterions surrounding them. A classical approach to the effective colloid-colloid interactions is based on the DLVO (Derjaguin Landau Verwey and Overbeek) model [31]. This model describes the effective-pair interaction between two charged colloidal particles in terms of a hard-core repulsion and Yukawa (screened Coulomb) repulsion, where the screening length is determined by the Debye length of the electrolyte. The screening length λ^{-1} is associated to the thickness of the double layer of opposite charges surrounding each colloid, and under some conditions (high concentration of electrolyte and/or low colloid volume fraction) charge-screened colloidal interactions are well described by the HCYM part of the DLVO model.

When we use the Yukawa screening parameter to describe the thickness of an electric double-layer, the HCYM becomes also relevant to describe electrolytes. Electrolytes are found even in human bodies where they regulate our nerve and muscle function, the hydration of our bodies, blood pH, blood pressure and they help in rebuilding the damaged tissues [32].

When there is a chemical binding, dissociation of chemical groups on the surface, chemical binding or physical adsorption of ions from the electrolyte, particles in polar solvents usually develop surface charges. Since the electrolyte is originally electroanal, the ions dissociated from the surface or the ex-partners of the adsorbed ions balance the surface charge. Although counterions are attracted to the oppositely charged surface due to entropy gain, they remain

dispersed and mobile in the solvent in the vicinity of the surface [33]. This physical situation having the layers of opposite charges can be modeled with an electric double layer. The electric double layer can be studied by adopting theories from the the foundations of classical statistical mechanics. The traditional approach is the Poisson-Boltzmann theory which is mean-field method: it takes the density of ions in the diffusive layer and makes it proportional to the Boltzmann factor of the average electrostatic potential [34].

The electric double layer dictates an inhomogeneous situation in the sense that ion density varies with the distance to the charged wall, in contrast to the bulk electrolyte where the ion density is uniform. As a result, the ion pair correlation functions depends only upon separation of the ions whereas in the double layer they depend on vector positions of the two ions. The bulk electrolyte and the double layer can be analyzed using some techniques, despite their quantitative differences. The bulk electrolyte determines many of the properties of the electric double layer, in particular the asymptotic decay of the density profiles and the interaction between overlapping double layers [34]. Understanding the structure and the adsorption of the electrolytes near a solid surface surface is relevant to many traditional applications such as gas storage, oil recovery and heterogeneous catalyst reactions [34]. The forces that exist between the confined particles themselves and with the solid surface are not easy to predict. The structure of fluids and their adsorption, wetting, etc. is obviously affected by the intermolecular interactions and the specific interactions between the fluid molecules and the adsorbate.

The need to understand equilibrium properties of electrolytes solutions, including thermophysical and chemical properties, fostered the development of theories used to predict such properties. With the advent of computers, sophisticated numerical techniques have become possible, including Monte Carlo (MC) and Molecular Dynamics (MD) computer simulation and integral-equation theories (IETs). For example, still focusing on applications in the field of electrolytes, simulations are even able to follow the motion of individual ions in the double layer, whereas integral equations are based on mathematical relationships between the ion density profile and the ion pair correlation functions, either those of the bulk electrolyte or those in the double layer. Another important theoretical approach is the density functional theory, which is based on a variational procedure to minimize the double layer free energy with respect to the ion density profile. Within this framework, the free energy of the system is approximated by assuming a fundamental relationship involving the bulk direct correlation function. DFTs are considered the theoretical method of choice for studying the adsorption of fluids.

1.2   Aims and Objectives

A basic simplification of most modern density functional theories (DFTs) as applied to classical fluids is to use a procedure to map the nonuniform (or nonhomogeneous) system into the uniform one [35, 36, 37, 38, 39, 40]. For instance, if we consider the pure HCYM alone, that is a model for

a uniform fluid, while when we consider it in the presence of a wall, the HCYM + the external potential created by the presence of the wall is the nonuniform system. Now, it is possible to make a formal trick and see the source of the spatial nonhomogeneity in space not as a wall (or whatever is the external potential acting on the particles of the system), but instead as generic "particle" of the system. If we assume that our system of particles is interacting with a pair potential $u^{(2)}(r_0^*)$, where r_0^* is the distance between two particles scaled by the natural length introduced by the interaction model (for the HCYM it is the diameter σ of the hard-core, so $r_0^* = r_0/\sigma$), then the external potential $w(\vec{r})$ will become the pair potential $u^{(2)}(|r_0 - \vec{r}|)$. It is interesting to note that within this framework, the nonuniform system is the uniform system itself so the one-body density distribution $\rho_w(\vec{r_1})$ of the nonuniform system, which is probably the most important correlation function we would like to know, is the uniform pair correlation function $\rho_0 g_0(|\vec{r_1} - \vec{r_0}|)$, where ρ_0 is the homogeneous density of the system, and g_0 is the well-known radial distribution function. The most important take-home message for us is that all the theories which can be applied to the nonuniform case, can now potentially be used also for the uniform case. The reason for that is related to the possibility to reverse this procedure. If we have a good theory for the homogeneous system and we know how to calculate $\rho_0 g_0(|\vec{r_1} - \vec{r_0}|)$, we can map this quantity into $\rho_w(\vec{r_1})$ and apply the same theory to all sort of different nonuniform situations where we may have a wall, a spherical cavity, a slit pore, and so on and so forth. Since a very widely adopted approach for studying the microscopic correlation functions of the homogeneous system is the one based on the so-called Integral-Equation Theories (IETs), which are based on coupling a formulation for the closure equation or a guess for the important bridge function $B_0(r_0^*)$ with the exact Ornstein-Zernike (OZ) equation of the homogeneous system, these "reverse engineering" approaches were called wall-particle OZ (WOZ) Integral Equation theories, or closure-based DFT [41, 42, 43, 44, 45, 46, 47]. One of the aims of this thesis was to work in this framework in this theoretical framework and find a proper theory to improve the predictions of these approaches with a special focus on the depletion. The latter is situation we have when a fluid adsorbed on a solid surface exhibits a number of particles smaller than the one far away from the surface (the *bulk* fluid), so the number density of particles near the wall (the contact density) is smaller than the *bulk* value (ρ_0, i.e. the density of the homogeneous fluid). On the contrary, when the contact density of the fluid is greater than ρ_0, we refer to this situation as adhesion. While WOZ IETs or closure-based DFTs proved to be reasonable describing the adhesive behaviour, they did not provide a similar performance in the treatment of the depletive cases [48, 49, 50].

Within the main aim of this research study, we would like to focus on the one-component HCYM in the presence of a hard-wall and apply a recent closure-based DFT approach that is based on higher-order correlation functions. The standard OZ equation involves a functional relationship between pair correlation functions of the fluid. We will use an approach based on the OZ3

equation, which involves a functional relationship between three-body (triplet) correlation functions. This approach was recently tested for the Lennard-Jones fluid [51], and it is important to generalize it to treat also the HCYM because of the existence of exact relationships for this system that can be potentially exploited to further improve the theory (hard wall sum rule). The two objectives we had in mind for this first part of the research were:

- Modify a numerical code for the OZ3-based DFT as applied to the case of the monocomponent LJ plus hard wall so to work for the case monocomponent HCYF plus hard wall.

- Test the wall-fluid correlation functions against exact Monte Carlo computer simulation data.

Then, the next aim would be the one of testing the theoretical approach for binary HCYM mixtures in the presence of a wall, so to consider a more realistic model for an electrolyte, where two charge-screened species (resembling the two oppositely charged species of an electrolyte) are exposed to a charge-screened wall. We would like to keep the theoretical treatment within the framework of charge-screened particles also because of the additional complication arising when taking into account the long-range Coulombic forces in both the theory and the computer simulation. Since there aren't many computer simulation data in the literature to test even the homogeneous case (i.e. homogeneous HCY mixtures), we have also to take care of generating our own Monte Carlo data. Then, the objectives as related to this aim were:

- Create from scratch a Monte Carlo code for the HCY binary mixtures and test it against results already published in the literature.

- Modify a numerical code for the OZ3-based DFT as applied to the case of the monocomponent LJ plus hard wall so to work for the binary HCY mixtures plus hard wall.

- Test the wall-fluid mixture correlation functions against exact Monte Carlo computer simulation data.

1.3 Overview

In this section we discuss briefly the main findings of the research we accomplished in our thesis, and at the end we will also provide a sketch of its structure.

Within the study of the HCYM in the presence of a wall, we firstly examined in general the expression of the Euler-Lagrange (EL) equations resulting from the minimization of the grand potential of a inhomogeneous fluid. The resulting equation coupled with the one that is defined in analogy with uniform fluids provides the general framework of the theoretical treatment of our system. The latter equation links the inhomogeneous indirect correlation function to the

inhomogeneous total correlation function and to the *homogeneous* direct correlation function provide the general framework of the theoretical treatment of our system. A key quantity to be determined was the bridge functional in the presence of the wall (external field), that is expressed as a functional of the indirect correlation function (still in the presence of the wall) and appears in the EL equation. Since there is a wall exerting an external force on the particles of the system, we are considering inhomogeneous correlation functions. Most of the well-known approximations for liquid-state theories consist in substituting the exact functional dependence of the bridge function on the indirect correlation function, with a function-type dependence (i.e. $B_w(\gamma(\vec{r_1}); \vec{r_1}) \approx B_w(\gamma(\vec{r_1})))$. The starting point for our approximation was the functional Taylor expansion in a number of infinite many-particle terms of the bridge functional in the presence of the wall, where the uniform (homogeneous) system is taken as a reference. Since this expansion is expected to the rapidly convergent, we retained the lowest term only, that is an integral of the homogeneous triplet direct correlation function of the system $C_0^{(3)}(1, 2, 3)$. Then, we performed an additional approximation for the expression of the three-particles direct correlation function, by using the exact third-order Ornstein-Zernike equation (OZ3). We set the triplet direct correlation function to zero, and by substitution inside the OZ3, we came to an expression for $C_0^{(3)}(1, 2, 3)$ that we named CAC3, that expresses $C_0^{(3)}(1, 2, 3)$ in terms of two-particle direct correlation functions. Reason for the choice of the name is that the formula obtained is mirroring a formula obtained by Jackson and Feenberg within the so-called convolution approximation, that can be obtained by substituting $C^{(3)}$ and $C^{(2)}$ (the two-particle direct correlation function) with $h^{(3)}$ and $h^{(2)}$ (the three- and two-particle direct correlation functions, respectively). The original formula was obtained to the purpose of studying the phonon-phonon interaction of a quantum fluid. The rationale for this approximation lays on the properties of recursion and normalization of the distribution functions which are preserved by the convolution approximation. When the CAC3 is used in the approximation for the bridge functional of the inhomogeneous fluid, an expression was obtained, named CA-OZ3 that clearly shows the presence of additional terms than one of most basic and widely adopted approximation, i.e. Percus-Yevick (PY) theory.

The next two steps were more dictated by phenomenological observations. The first one was to substitute the only term reported in CA-OZ3 and related to the PY theory with the one provided by a more sophisticated theory, the ZSEP (Zero-Separation theory), that possesses as a remarkable property the one of satisfying some exact statistical-mechanical identities called zero-separation theorems. Since the latter determine the behaviour of correlation functions at short-distance, we deemed ZSEP as a proper approach for fluids in the presence of a wall. Finally, we made use of a procedure called renormalization for the *homogeneous* direct correlation function appearing in the equation mentioned at the beginning, which links the inhomogeneous inverse and direct correlation functions. Within this framework, we substituted in both the ZSEP and the CA-OZ3 the pair indirect and direct correlation functions, which are obtained by

assuming that the pair correlation function vanishes for distances greater than the hard-sphere diameter of the HCY model. The rationale for his choice is the empirical observation by inverting computer simulation data within these equations that the inhomogeneous bridge functional becomes more similar to a function of the indirect correlation function.

The new theoretical framework briefly described above is named CA-OZ3, and it was successfully implemented for the first time in the study of the Lennard-Jones fluid model in the presence of a hard-wall. In our thesis, we originally adapted this approach to study the HCYM in the presence of a hard-wall. Our results, preliminary preceded by the technical details of the theory, are reported in Chapter 3 and compared against Monte Carlo data available in the literature.

In the second part of our research activity, we focused on the binary mixture model. While our initial aim was to consider it in the presence of a hard-wall, we quite soon realized the scarcity of computer simulation data available in the literature for it. Even for the homogeneous system, the most recent data available were dated back to the early nineties, so we refrained from extending the model to the inhomogeneous case and we worked on the production of novel Monte Carlo (MC) data with a new code we developed to that aim in order to provide a more recent and reliable benchmark for the theoretical calculations. This endeavour was extremely rewarding because it allowed us to detect some serious issues in the MC data already published and allowed us to conclude that they were affected by finite-size problems. In other words, the system sizes considered in those articles were so small that the thermodynamic quantities obtained as statistical averages in the simulations were size-dependent, and not providing a reliable estimate to assess theoretical approaches. This situation was made even worse by the awkward choice of energy potential parameters for the two species, that was favoring phase separation in the system due to the enhanced self-attraction induced in one of the two species. The picture emerging from our analysis was recognized to be quite problematic, especially because in the last twenty-five years a number of statistical-mechanical theories reported in the literature for binary HCYMs have been assessed against those data. Our results are reported and compared with those already published in the scientific literature in Chapter 4, while an introduction to the Monte Carlo computer simulation approach comes before it.

Finally, in Chapter 5 we conclude with some remarks about what we achieved and some outlook on the perspectives that our work opened for further studies.

Chapter 2

Literature Review

2.1 The Hard-core Yukawa fluid

The hard-core Yukawa model has been one of the most studied pair potentials in the literature related to liquid state theory because of its ability to exhibit a number of properties of real fluids. This is achieved by simply varying the interaction range [52]. The Yukawa model is a three-parameter model: the parameter ϵ (the energy depth), the parameter σ (the particle diameter) and the parameter λ (the screening parameter). This model can be studied by making it to represent an attractive or a repulsive pair potential just by changing the sign which multiplies the energy depth. Most of the research done on the hard-core Yukawa model was based on the attractive Yukawa potential. Theories and computer simulation have been widely employed to study the thermodynamic and diffusion properties of the fluids represented by this model. Just to mention a few of them, the HCYM was applied to simple neutral fluids [53, 54, 55, 56], chain-like fluids [57, 58], liquid metals [59], charge-stabilized colloids [60], dilute solution of strong electrolytes [61], globular proteins [62], fullerenes [63] and hydrogen [64]. The full phase behaviour of hard-core attractive Yukawa (HCAY) fluid was determined by Dijkstra [65], who obtained it by calculating the Helmholtz free energy as a a function of the density by using thermodynamic integration. Gonzalez-Melchor *et al.* studied the interfacial properties of the liquid-vapor interface by applying a hybrid molecular dynamic algorithm [66]. Shukla calculated the vapor-liquid phase diagram of the HCAY fluid and he was the first person to state a caution about finite size effects possibly hampering computer simulation studies of this model [67].

The hard-core Yukawa model was also applied to model inhomogeneous (confined) fluids. In predicting the density profile of an inhomogeneous HCY fluid near a hard wall, Olivares-Rivas *et al.* [49] used the singlet hypernetted chain (HNC) integral equation and a modified version of the Lovett-Mou-Buff-Wertheim (LMBW-1). Their predictions were done at a reduced density $\rho\sigma^3 = 0.7$ and they showed a better performance of LMBW-1 equation at high temperatures

while at low temperatures it overestimated the density profiles. Soon after, based on the density functional approximation of Rickayzen *et al.* [68, 69] and the weighted-density approximation (WDA) of Tarazona [70, 71], Yi and Kim [72] had a proposal of a density functional perturbative approximation for the attractive attractive HCY fluid. You *et al.* [73] reformulated the Helmholtz free-energy function through Rosenfeld's perturbative method [59] for the inhomogeneous attractive and repulsive HCY fluid. They then applied the theory to investigate the density profiles of these types of fluids near a wall, and also to find the radial distribution functions of the homogeneous HCY fluid.

The studies done on inhomogeneous attractive hard-core Yukawa are for $1.8 \leq \lambda \leq 7.0$ and most of them are limited at $\rho\sigma^3 = 0.7$. A powerful tool to study the structural properties of inhomogeneous fluids is the density functional theory (DFT), though there is no exact form for the Helmholtz free-energy functional, and approximations for it are commonly adopted [73]. The advantage of working with a simple model like the HCYM, is that it can be used to test the development and/or improvement of many theories.

Henderson, Abraham and Barker [46] used Percus-Yevick (PY) approximation for hard spheres near a hard wall, and they developed the singlet integral equation approach for inhomogeneous fluids. Following this achievement, systematic extensions of the Poisson-Boltzmann theory for an electric double layer followed [74]. The liquid-vapor phase stability of the one component HCYF was investigated by Cummings and Smith [75], Cummings and Stell [76] by using the Mean Spherical Approximation (MSA). They considered a system with λ=7.5 and found the critical point to occur at k_{cr}=5.033605 and η_{cr}=0.245011, where η is the packing fraction ($\eta = (\pi/6)\rho\sigma^3$) and k is the inverse of the thermodynamic temperature in units of the Boltzmann constant. Henderson *et al.* [77] also found a good agreement between the Monte Carlo (MC) simulation data and the results obtained from a thermodynamic model for the HCYF based on the MSA [78]. The HCYF freezing line was also determined through density functional theory [79, 80], and the binodal (liquid-vapour) line has been determined by Smit and Frenkel [81] through Gibbs ensemble Monte Carlo simulation.

2.2 Computer simulation of binary, hard-core Yukawa mixtures

You, Yu and Gao [73] carried out grand canonical ensemble Monte Carlo (GCMC) simulations to obtain the density profile of asymmetric binary HCY fluid mixtures in a slitlike pore. Their simulations were carried out for different temperatures, different energy parameters, diameter ratios, *bulk* mole fractions and densities. The focus of their research was to test some DFT predictions [73] and investigate whether the mean field (MF) approximation still holds when the fluctuations of the order parameters of the liquid-vapor (LV) and of the demixing transitions are taken into account. Patra and Smith [82] applied a self-consistent DFT to a binary attractive hard-core Yukawa mixture to reproduce the simulations results by You *et al.* [73]. Pini *et al.* [83] applied the hierarchical reference theory (HRT [84]) to a hard-core Yukawa fluid mixture (HCYFM) and their findings showed a persistence of the intermediate type II phase diagram [85] up to the size ratio of $\alpha = 0.8$, at which it is possible to get a reliable solution of the HRT. Scholl-Paschinger *et al.*[85] aimed on establishing the accuracy of the self-consistent Ornstein-Zernike approximation (SCOZA) and HRT theoretical approaches by performing MC simulations of the equimolar HCYFM model. They further investigated the effect of increasing the Yukawa potential range on the phase diagram. They found that the SCOZA theory performs better as the range of the Yukawa potential increases. Finally, the structural behaviour of binary attractive and repulsive HCY mixtures near a model for a semi-permeable membrane was investigated by Z. Yang *et al.* [86] by using a DFT approach which is a combination of the Kierlik-Rosinberg Weighted density approximation (WDA) and the MF approximation.

When we looked at the symmetric HCYFM, where the diameters of the two species are equal to each other, we were able to find a few papers only. Rey *et al.* [9, 87] performed molecular dynamics (MD) computer simulations to get an insight about the structure and the thermodynamic properties of real fluids. In their study they focused on additive (the crossed diameter of the interaction between different species is equal to the arithmetic average) and nonadditive hard-core Yukawa equimolar mixtures. When they compared their MD results with the MSA results, they observed a good agreement at lower densities and at higher densities they observed some discrepancy for $\Delta = 0.1$.

Chapter 3

Hard-core Yukawa fluid in the presence of a hard wall

3.1 Introduction

Hardcore Yukawa model is one of the models that can be used to study the behaviour of fluids. Because of its flexibility and versatility, it can be used to study the simple fluids and also the complex ones by simply changing the inverse screening length. The research on the adsorption, interfacial tension and wetting of fluids near planar or curved walls has gained a lot of attention because of the potential industrial applications of these properties in membrane transport, chromatography and lubrication. In engineering, the interfacial tension is applicable in mass transfer operations, filtration and thermal conductivity of nanofluids. These properties will differ for planar surfaces as compared to the curved surfaces since they depend on the wall curvature and geometry.

The nature of the fluid affects its behaviour near a surface, this is due to the orientational ordering. Nematic fluids show richer behaviour near a surface than simple fluids. There is a variety of approaches that are taken in studying the behaviour/properties of confined fluids, a few of these approaches are experimental designs, computer simulations and density functional theory. Systems that interact with a Yukawa like potential are of great interest in the theoretical research. We can easily study the thermodynamic properties and the structure of the Yukawa fluid because of the simplicity of the Yukawa potential.

The potential due some interacting point particles within a finite range from each other can be decomposed to a sum of Yukawa potentials with arbitrary accuracy. There has not been much research conducted on non-uniform systems of particles interacting with a Yukawa potential as there has been for spatially uniform Systems. From the known fluid particle distribution function calculated from the bulk system, we can calculate the fluid particle distribution function for the

very same system but in the presence of the wall this time. This leads to the calculation of the fluid density profile whose calculation reduces to the solution of the Ornstein-Zernike integral equation. There are some known exact relationships, like sum-rules, that need to be satisfied by the results of the spatially non-uniform systems. With the help of computer simulations and numerical calculations of integral equations, our understanding of surface effects in systems confined by a hard wall has been broadened. In the following section we will focus on how fluids with a Yukawa potential behave in the presence of a hard wall.

3.2 Theory of the third-order Ornstein-Zernike equation

Ornstein-Zernike (OZ) equation is a statistical mechanical integral equation named after Leonard Ornstein and Frits Zernike used to describe the calculation of the statistical correlation between two particles:

$$h(r_{12}) = c(r_{12}) + \rho \int d\mathbf{r}_3 c(r_{13}) h(r_{23}) \tag{3.1}$$

The total correlation function $h(r_{12})$ between particle 1 and particle 2 when they are at a distance r_{12} far apart is defined as

$$h(r_{12}) = g(r_{12}) - 1, \tag{3.2}$$

where $g(r_{12})$ is the radial distribution function. The other unknown function is $\gamma(r_{12}) = h(r_{12}) - c(r_{12})$, where $c(r_{12})$ is the direct correlation function. In fluid theory, to obtain the radial distribution functions we have to cope the OZ equation with another equation establishing a functional relationship between $h(r_{12})$ and $c(r_{12})$, like in the case of the Percus Yevick (PY) [88] and hypernetted-chain (HNC) [89] equations, for example. In 1914 Ornstein came with a proposal [90] to decompose the total correlation function into a direct and an indirect part, with the direct part being the direct correlation between particles 1 and 2 and it is denoted by $c(r_{12})$ as we already reported above, and the indirect correlation function (icf) $\gamma(r_{12})$ being a result of the influence that molecule 1 has on a third molecule (molecule 3) in the system; this influence has a direct and also an indirect effect on molecule 2. The indirect correlation function $\gamma(r_{12})$ is weighted by the density (ρ) and averaged over all the possible positions of particle 3 according to the OZ equation reported before; the latter can also be written as

$$\gamma(r_{12}) = \rho \int d\mathbf{r}_3 c(r_{13}) h(r_{23}) \tag{3.3}$$

NOTE: In this dissertation any quantity with a subscript $_0$ is a homogeneous quantity, the subscript $_w$ on any quantity denotes an inhomogeneous quantity. The superscript $^{(i)}$ (i=2,3,4,...) on any quantity denotes the i-th order.

As much as there are computer simulations which can be performed to some degree of accuracy to predict the properties of some models, there is still a need for theories to be built, or modified. Simulations are performed to test some theories, and if their results agree well with the theory for the model under consideration, then the theory can be potentially extended to even more sophisticated models, for which computer simulations might be time consuming, if achievable in a reasonable computational time at all.

For an N-body system under influence of an external one-body potential $w^{(1)}$, the Hamiltonian H_N is given by

$$H_N(p^N, r^N) \equiv \sum_{i=1}^N \frac{p_i^2}{2m} + \sum_{i=1}^N \sum_{<j}^N u^{(2)}(r_{ij}) + \sum_{k=1}^N w^{(1)}(r_k), \tag{3.4}$$

where p^N is the N-vector of momenta, r^N the N-vector of positions, m = mass of molecules, $u^{(2)}$ is the pair potentials among the fluid particles. r_{ij} is the relative distance $|\vec{r}_j - \vec{r}_i|$. $\vec{r}_k$ is the kth molecule. The commonly known second-order OZ equation

$$h_0^{(2)}(1,2) - C_0^{(2)}(1,2) \equiv \int d3 C_0^{(2)}(1,3) \rho_0 h_0^{(2)}(3,2) \tag{3.5}$$

can be shown to result from the inverse relation of the fluctuation derivative and compressibility derivative (as in the functional calculus of Lebowitz and Percus) [91]

$$\int d3 \frac{\delta \rho_w(1)}{\delta W(3)} \frac{\delta W(3)}{\delta \rho_w(2)} = \delta_3(1,2) \tag{3.6}$$

where W is the intrinsic chemical potential defined by: $W(\vec{r}) \equiv \beta \mu_0 \beta w^{(1)}(\vec{r})$. (Notation: arguments $1 = \vec{r_1}$, and $2 = \vec{r_2}$, etc.), and $\delta_3(1,2)$ is the three dimensional Dirac delta function. Note that h is the total correlation, C the direct correlation. $\beta \mu_0$ is the bulk chemical potential divided by kT (μ_0/kT): k = Boltzmann constant and T = absolute temperature. The functional derivatives are known explicitly from Lebowitz and Percus [91]

$$\frac{\delta \rho_w(1)}{\delta W(2)} = \delta_3(1,2) \rho_w(1) + F^{(2)}(1,2) \text{ and}$$
$$\frac{\delta W(1)}{\delta \rho_w(2)} = \frac{\delta_3(1,2)}{\rho_w(1)} - C^{(2)}(1,2) \tag{3.7}$$

where $F^{(2)}$ is the Ursell distribution function. Naturally, we can inquire about the relations among the higher functional derivatives. This has been done previously [92], and we shall cite only the results here. There are six equivalent forms of the third-order OZ relation. The one that we are interested in is the functional relation

$$\frac{\delta^2 W(1)}{\delta \rho_w(2) \delta \rho_w(3)} = - \int d4 d5 d6 \frac{\delta W(4)}{\delta \rho_w(3)} \frac{\delta W(6)}{\delta \rho_w(2)} \times \frac{\delta W(1)}{\delta \rho_w(5)} \frac{\delta^2 \rho_w(5)}{\delta W(4) \delta W(6)} \tag{3.8}$$

After some algebra, we obtain the OZ3 equation [91]

$$C_{123} = h_{123} - C_{12}C_{13} - C_{21}C_{23} - C_{31}C_{32}$$
$$- \rho^3 \int d4d5d6 C_{14}C_{25}C_{36}h_{456}$$
$$+ \rho^2 \int d5d6 C_{15}C_{26}h_{356} - \rho \int d5 C_{15}h_{235}$$
$$+ \rho^2 \int d4d5 C_{15}C_{34}C_{36}h_{245} - \rho \int d6 C_{26}h_{136}$$
$$+ \rho^2 \int d4d6 C_{26}C_{34}h_{146} - \rho \int d4 C_{34}h_{124}$$
$$+ 2\rho \int d4 C_{14}C_{24}C_{34}$$

(3.9)

NOTE: In the above equation the number of digits in the subscript denotes the order of the quantity, and the numbers represented in the subscript denotes the interacting particles. In equation(3.9), we we dropped the superscripts and subscript 'w' to save space. Form equation(3.9) is exact. However, it is difficult to be implemented because of the higher order correlations contained therein. In Ref. [51], we simplified OZ3 by using a convolution approximation (CA) similar to that of Jackson and Feenberg [93] by setting $h^{(3)} \sim 0$. Thus

$$C^{(3)}(1,2,3) \cong -C^{(2)}(1,2)C^{(2)}(1,3)$$
$$- C^{(2)}(2,1)C^{(2)}(2,3) - C^{(2)}(3,2)C^{(2)}(3,1)$$
$$+ 2\rho \int d4 C^{(2)}(1,2)C^{(2)}(2,4)C^{(2)}(3,4). \text{ (CA-OZ3)}$$

(3.10)

This is a simplified version of the OZ3 equation by using the Convolution Approximation (CA-OZ3). This appears to be a drastic approximation for $h^{(3)}$. Other milder and possibly better approximations for the triplet total correlation functions $h^{(3)}$ can also be made (see [94]), and such will be investigated in the future.

3.3   Constructing the bridge function with aid of the OZ3 equation

Realizing the poor performance of the traditional PY and HNC closures, we intend to construct a more accurate closure. First, we should recognize that any DFT that contains or implies the EulerLagrange equation (EL) postulates bridge function, either consciously or unconsciously, even though the particular approach was not based explicitly on bridges. The EL we are referring to is the equation [95, 96, 97]

$$\rho_w(\vec{r}) = \rho_0 exp[\ -\beta w^{(1)}(\vec{r}) + C_w^{(1)}(\vec{r})\ -\ C_0^{(1)}],$$

(3.11)

Where $C_w^{(1)}(\vec{r})$ and $C_0^{(1)}$ are the singlet direct correlation functions, s-dcfs (subscript w indicates the non-uniform system, while 0 indicates the uniform system). The s-dcf is defined as the derivative of the excess free energy, F^{ex}, i.e.

$$-\frac{\delta \beta F^{ex}[\rho]}{\delta \rho_w(r)} \equiv C_w^{(1)}(r). \tag{3.12}$$

In our approach, the bridge function B_w is defined in the following ways

$$\rho_w(\vec{r}) \equiv \rho_0 exp[\ -\beta w^{(1)}(\vec{r}) + \gamma_w(\vec{r}) + B_w(\vec{r})]. \tag{3.13}$$

Thus we have the identity

$$C_w^{(1)} - C_0^{(1)}(\vec{r}) = \gamma_w(\vec{r}) + B_w(\vec{r}), \tag{3.14}$$

where the indirect correlation function $\gamma_w(\vec{r})$ (icf) is defined as the convolution integral

$$\gamma_w(\vec{r}) \equiv \int d\vec{r'} C_0^{(2)}(|\vec{r} - \vec{r'}|) \delta \rho_w(\vec{r'}) \tag{3.15}$$

in analogy with the icf in uniform fluids, where $\delta \rho_w(\vec{r}) \equiv \rho_w(\vec{r}) - \rho_0 \equiv \rho_0 h_w(\vec{r})$ and $h_w(\vec{r})$ is the non-uniform total correlation function. Thus, if the DFT admits an EL equation (i.e. with an obvious expression for $C_w^{(1)}(\vec{r})$), then through Equation (3.14), we can extract the form of the bridge function for this DFT. This actually has been carried out by Rosenfeld and co-workers [98] in the FMT approach for hard spheres on an HW. A similar extraction can be made for a bridge function in the local molecular field approach of Rogers and Weeks [99] by applying Equation (3.14). Here it is opportune to remark on our usage of the terms (1) the bridge function (or bridge functional) and (2) the closure relation. (1) A bridge function B_w is a well-defined quantity in statistical mechanics (either through the cluster integrals, or by eq. (3.14)). It exists, as remarked earlier, as a legitimate correlation function, just as the s-dcfs. (2) On the other hand, the closure relation is a theory, expressed as an equation that relates other correlation functions (such as the icf, $\gamma_w(\vec{r})$) to the bridge function $B_w(\vec{r})$. This equation $B_w = \Phi[\gamma_w]$ may or may not be exact. In fact, in almost all cases, it is an approximation. The symbol Φ can be a function relation, or can be a functional. The closure-based DFT is an attempt to construct an equation, Φ, that hopefully will give a good representation of the bridge function in the particular application. It is also known that the bridge functional admits an expansion in terms of the higher order (uniform) direct correlation functions [100]

$$B_w \equiv \frac{1}{2!} \int d2d3 C_0^{(3)}(1,2,3)\delta\rho_w(2)\delta\rho_w(3)$$
$$+ \frac{1}{3!} \int d2d3d4 C_0^{(4)}(1,2,3,4)\delta\rho_w(2)\delta\rho_w(3)\delta\rho_w(4)$$
$$+ \frac{1}{4!} \int d2d3d4d5 C_0^{(5)}(1,2,3,4,5)\delta\rho_w(2)\delta\rho_w(3)\delta\rho_w(4)\delta\rho_w(5) \qquad (3.16)$$
$$+ \frac{1}{5!} + ... + \frac{1}{6!} + ...$$
$$= B_3 + B_4 + B_5 + B_6 + ..., \text{ respectively,}$$

where $C_0^{(n)}$ $(n = 3, 4, ..., n)$ are the uniform nth-order direct correlation functions. Since we have obtained an expression (3.10) for the third-order dcf, the B_3 term can be approximated (in the CA-OZ3 approximation) as

$$B_3(1) \cong -\frac{\gamma_w(1)^2}{2} - \rho_0 \int d2 C_0^{(2)}(1,2)\gamma_w(2)\delta\rho_w(2)$$
$$+ \rho_0 \int d2 C_0^{(2)}(1,2)\gamma_w(2)^2. \qquad (3.17)$$

This equation expresses B_3 both as a function and as a functional of the icf γ_w. We shall use this insight as the basis for constructing a full bridge functional. Upon considering (as in Ref [51]) that the higher order bridge terms B_4, B_5, etc. assume similar forms as (3.17), we arrive at the following more complete expression

$$B_w \cong -\frac{\zeta\gamma_w(1)^2}{2}[1 - \phi + \frac{\phi}{1 + \alpha\gamma_w(1)}]$$
$$- \psi\rho[\int d2 C_0^{(2)}(1,2)\gamma_w(2)\delta\rho_w(2) \qquad (3.18)$$
$$- \int d2 C_0^{(2)}(1,2)\gamma_w(2)^2],$$

where ζ, ϕ, α, and ψ are parameters to be determined from the state conditions. As explained earlier [51], the icf s should be renormalized to avoid multi-valued functions (or more precisely to convert a functional into a function), a new icf γ_H is defined

$$\gamma_H(\overrightarrow{r}) \equiv \int d\overrightarrow{r'} C_H^{(2)}(|\overrightarrow{r} - \overrightarrow{r'}|)\delta\rho_w(\overrightarrow{r'}) \qquad (3.19)$$

where

$$C_H^{(2)}(r) \equiv \begin{cases} C_0^{(2)}(r), & \text{for } r \leq \sigma; \text{ and} \\ 0, & \text{for } r > \sigma. \end{cases} \qquad (3.20)$$

Therefore, the end product is the following renormalized closure for the bridge function

$$B_w \cong -\frac{\zeta\gamma_H(1)^2}{2}[1 - \phi + \frac{\phi}{1 + \alpha\gamma_H(1)}]$$
$$- \psi\rho[\int d2C_0^{(2)}(1,2)\gamma_H(2)\delta\rho_w(2)$$
$$- \int d2C_H^{(2)}(1,2)\gamma_H(2)^2]$$

(3.21)

(the renormalized - OZ3 equation).,

We shall apply this closure to the adsorption of the HCAY fluid.

3.4   inhomogeneous Yukawa fluid

In the most researches that have been carried out on hard-core Yukawa fluids (HCY), the studies were limited to the pure attractive and repulsive HCY fluids. The key focus of the investigations were the pair correlation functions, phase equilibria, thermodynamic properties and the surface tension. Some of the theories that are mostly employed when conducting such researches are the integral equation theories (IET), perturbation theory and also Monte Carlo simulations. So far the investigations on the inhomogeneous attractive HCY fluids are limited to the reduced density $\rho^* = 0.7$.

When fluids adsorb on a hard wall, we observe one of the following situations with regard to the singlet density function:

1. There is a higher contact density value than the bulk density. This is a case when there is an additional number of molecules at the wall, this situation is called *adhesion*.

2. There is a less contact density value than the bulk density. This happens when there is a deficit of molecules at the wall. This is called *depletion*.

3. There can can also be an even distribution.

In statistical mechanics, the density profile near and not far from the wall is described by the singlet probability density $\rho_w(z)$ (z being the distance normal to the wall). Far from the wall $(z \to \infty)$, $\rho_w(z)$ approaches the constant bulk density value ρ_0. Adhesion or depletion of molecules near the solid substrate is a general behaviour: present at either supercritical or subcritical states, with different substrate affinities, molecular species, and geometries of the inhomogeneities. Accumulation or detachment of molecules at the interface is the result of competition between the interfacial wall forces and the coherent fluidfluid forces among the fluid molecules vis--vis the state conditions (phase diagrams, pressures, and temperatures, see the reviews [101, 102]). It is the charge of the statistical mechanics discipline to delineate the interplay amongst these factors. Compared to the weighted-function approaches [103] in the density functional theory (DFT) for inhomogeneous fluids, the conventional closure-based integral

equations (based on an approximate bridge function or functional) have been less successful in dealing with the depletion adsorption. In a previous theoretical development [51] (see Ref. [51]), we have proposed a new formulation, the Ornstein-Zernike (OZ3) based closures for the bridge function (closures based on the OZ3 equations). An early test on the depletive adsorption of the Lennard-Jones fluid on a hard wall (HW) showed promise [51]. In this study, we shall further examine the adsorption of another simple fluid, exemplified by the hard-core attractive Yukawa potential (HCAY), on a simple HW. We shall pay special attention to cases of the depletive adsorption, precisely because these systems are more difficult to describe by the analytical theories. The traditional closures for uniform fluids, such as the PercusYevick (PY) and hypernetted-chain (HNC) equations, fall short to give quantitative answers for these non-uniform cases, as we shall see in detail in the next sections. There have been a number of studies on the Yukawa fluid/hard wall (Yu/HW) systems [49, 73, 104, 17, 105, 82]. While the approaches based on the fundamental measure theory (FMT [103]) have been quite accurate, attempts made employing the closure-based DFT have not yielded equally successful results for depletive absorptions. We shall test and ascertain the performance of the present OZ3-based bridge functions for the Yu/HW systems. The theoretical basis has been laid out in Ref. [51]. Therefore, we shall be brief on the details of this approach. Section 2 gives an overview of the OZ3 equation. In Section 3, we outline the construction of the third-order term in the bridge functional expansion and the rationale to generalize it to higher order terms. We apply the new bridge functional to the attractive Yukawa fluid adsorbed on an HW in Section 4. Five state conditions are examined. Most cases show the depletion type of adsorption. To determine the validity of the present approach, we also performed new Monte Carlo (MC) simulations for this non-uniform system in the constant number (N), volume (V), and temperature (T) ensemble (i.e. NVT).

3.5   Results and Discussion

The hard-core attractive Yukawa fluid has the pair potential

$$u^2\left(r^*\right) = \left\{ \begin{array}{l} +\infty,\ \text{for } r^* < 1 \\ -\epsilon \frac{e^{-\lambda\left(r^*-1\right)}}{r^*},\ \text{for } r^* \geq 1 \end{array} \right\} \tag{3.22}$$

where ϵ and σ are the energy and size parameters of the potential, $r^* = \frac{r}{\sigma}$. We study two cases of the range parameter λ, namely at 1.8 and 3. The value $\lambda = 3$, in combination with the chosen temperature and densities, gives us the depletive adsorption as observed in the MC calculations. The value $\lambda = 1.8$ is for comparison with literature DFT data. The planar structureless hard wall is located at $\frac{\sigma}{2}$

$$w^{(1)}\left(r\right) = \left\{ \begin{array}{l} +\infty,\ \text{for } r < \frac{\sigma}{2} \\ 0,\ \text{for } r \geq \sigma \end{array} \right\} \tag{3.23}$$

We shall examine five state conditions: three cases at $\lambda = 3$, reduced temperature $T^* = 0.76$ and reduced densities $\rho^* = 0.358$, 0.473 and 0.557; and two cases at $\lambda = 1.8$ and reduced temperatures $T^* = 1.25$, and 2.0 with reduced density $\rho^* = 0.7$. Most of these states have shown depletive behavior at the hard wall. Thus this poses a stringent test of the theory. The bridge function is applied to all cases and the parameters ζ, ϕ, α and ψ are allowed to vary until (i) they satisfy the hard-wall sum rule below; and (ii) reproduce as closely as possible the MC singlet density profiles. The hard-wall sum rule is

$$\rho_w \left(z = \frac{\sigma}{2} \right) = \frac{P_0}{kT} \tag{3.24}$$

where P_0 is the bulk fluid pressure, that can be obtained independently from MC data or from an accurate integral-equation theory for the homogeneous system. We list in Table (3.1) (i) the values of P_0 obtained from integral-equation theory, (ii) values of the contact density $\rho_w \left(z = \frac{\sigma}{2} \right)$ from the MC simulation; and (iii) the contact density from the CA-OZ3 closure. The parameters used in the closure are given in Table (3.2).

In order to supply the homogeneous structural function $C_0^{(2)}$ for the EL equation, we used three closure theories: the PY, the modified hypernetted-chain (MHNC), and the zero-separation closure (ZSEP) closures via the homogeneous OZ equation:

$$\gamma_0^{(2)} (r) \equiv \rho_0 \int dr' C_0^{(2)} \left(|\, \vec{r} - \vec{r'} \,| \right) h_0^{(2)} \left(r' \right) \tag{3.25}$$

These closures provide additional relations linking the structural functions, whose general form is

$$1 + h_0^{(2)} (r) = exp \left[-\beta u^{(2)} (r) = \gamma_0^{(0)} (r) + B_0^{(2)} (r) \right] \tag{3.26}$$

where $B_0^{(2)} (r)$ is the homogeneous bridge function, whose specific formulation depends on the selected closure. For the MHNC closure, we input the bridge function of the hard spheres, and the hard-sphere diameter was used as a free parameter, as usual, to satisfy the thermodynamic consistency in the properties.

We start by considering the CA-OZ3-based closure at a moderate reduced density $\rho^* = 0.358$. Since we wanted to understand the effects of different inputs from the homogeneous-fluid direct correlation function $C_0^{(2)} (r)$ on the solution, we chose both the PY $C_0^{(2)} (r)$ and MHNC $C_0^{(2)} (r)$ as examples and gauged their influences on the eventual non-uniform density profiles $y_w (z^*)$.

In Figure (3.1), we compare these results for the inhomogeneous cavity function $y_w (z^*)$ with MC computer simulation. We clearly see that the theoretical structural functions are quantitative for reduced distances $z^* > 2$, while they are slightly deviating from the MC data at lower z-distances where the cavity function develops anon-monotonic change in its slope. Overall, the two different homogeneous inputs (PY and MHNC [106]) provide a comparable performance, with the exception of the MHNC one, that apparently develops a curious hook at distances very close to the wall ($z^* \cong 0.5$). We will try to provide some insight into this feature later. Increasing the density to $\rho^* = 0.473$ does not seem to change the overall agreement significantly (Figure

Figure 3.1: Inhomogeneous cavity functions as a function of the distance from the wall for $\rho^* = 0.358$
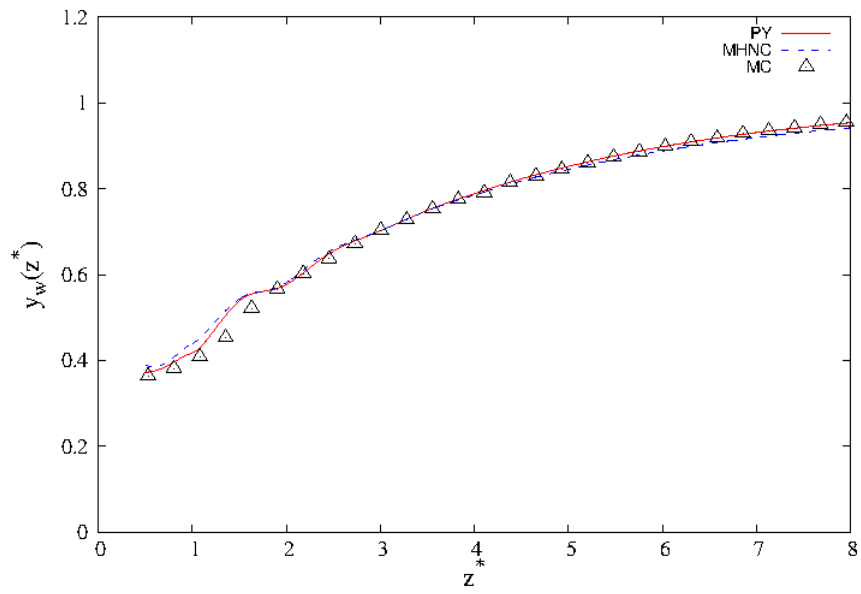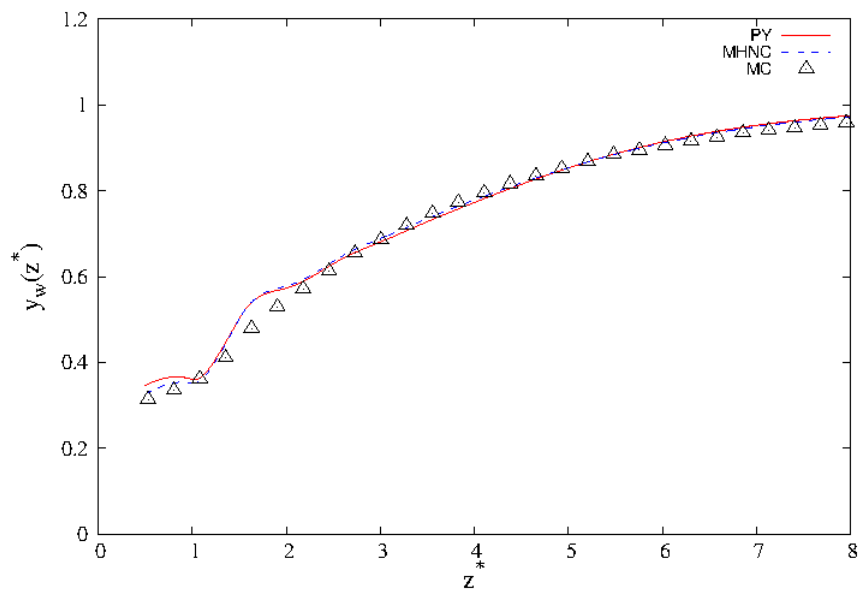

Figure 3.2: Inhomogeneous cavity functions as a function of the distance from the wall for $\rho^* = 0.473$

(3.2)), with a peculiar behaviour observed at short distances similar to the case considered before (Figure (3.1)).

Figure 3.3: Inhomogeneous cavity functions as a function of the distance from the wall for $\rho^* = 0.557$
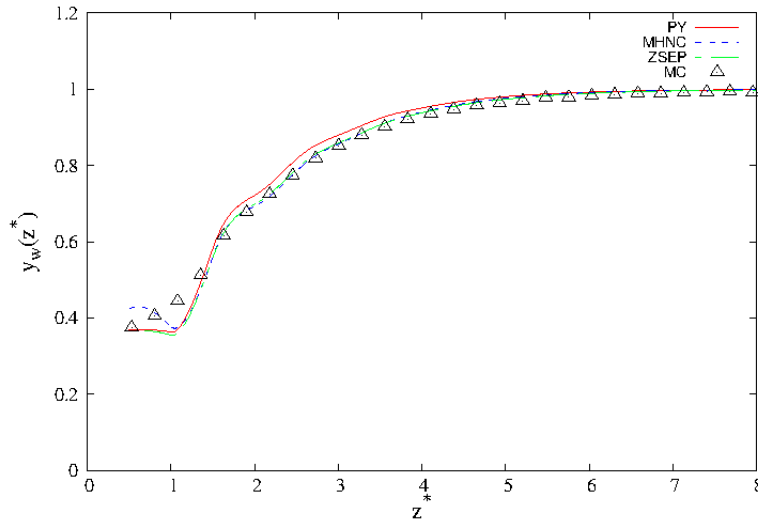
Next, in Figure (3.3), we report the calculations at the density $\rho^* = 0.557$ with both PY and MHNC as homogeneous $C_0^{(2)}(r)$ inputs. For this case, we also report results from the so-called ZSEP closure [107, 108] for $C_0^{(2)}(r)$. Overall, the calculations performed from $C_0^{(2)}(r)$ derived from the MHNC and ZSEP appear to be in better agreement with the MC data. Once again, at short distances, all theoretical inputs show deviations from MC, with a hook particularly pronounced in the MHNC-derived $C_0^{(2)}(r)$.

In order to gain some insight into this discrepancy vis-à-vis the MC data, we further compared the inhomogeneous bridge functions from CA-OZ3 and from inversion of the MC data, by using the defining equation: $B_w(z) = \ln y_w(z) - \gamma_w(z)$, in such manner that the cavity function $y_w(z)$ was obtained directly from the MC computer simulations, and the indirect correlation function $\gamma_w(z)$ was calculated from Equation $\gamma_w(\vec{r}) \equiv \int d\vec{r'} C_0^{(2)}(r)\left(\mid \vec{r} - \vec{r'} \mid\right)\delta\rho_w(\vec{r})$ by using the inputs $\rho_w(z)$ from MC and $C_0^{(2)}(r)$ from one of the selected uniform closures. Results are reported in Figure (3.4). If we examine the behaviour of the theoretical bridge functions $B_w(z)$ (CA-OZ3), they drop to zero slopes when approaching the wall (at $z = 0.5$), i.e. at the contact distance. On the other hand, the MC bridge function $B_w(z)$ reported in Figure (3.4) does not show such flattening near $z = 0.5$. $B_w(z)$ (MC) terminates at $z = 0.5$, as MC simulation should, not to penetrate into the HW. The theoretical $B_w(z)$ (CA-OZ3) can, of course, enter the wall due to the removal of wall potential in the cavity function $y_w(z)$, just as in the uniform case.

Thus, the inversion trend in the cavity function $y_w(\vec{r})$ (the hooking behaviour) is a reflection of the $B_w(z)$ (CA-OZ3) behaviour. Even though this appears to be a theoretical problem, it is

Figure 3.4: Inhomogeneous bridge functions as a function of the distance from the wall for $\rho^* = 0.557$
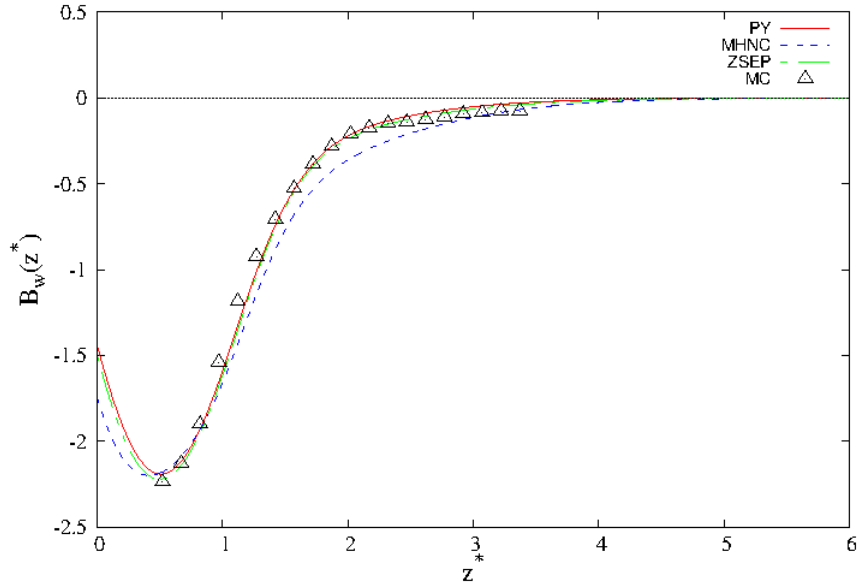
worth comparing what would happen when the PY and HNC theories were applied here as the non-uniform closures. In Figure (3.5), we show the calculation [106] done at $\rho = 0.557$ by using the non-uniform PY and HNC bridge functions (obviously, $B_w(\vec{r}) = 0$ in the HNC case). It is evident that these theories fail to reproduce even qualitatively the MC profile (the MC data are reported as triangles in Figure (3.5)). Both PY and HNC show oscillatory behaviour as a function of the distance and clearly overestimate MC data. In fact, PY and HNC predict adhesive adsorption when approaching the wall, a wrong behaviour. These observations are contrary to the depletive adsorption as shown by the MC data. The MC $y_w(z_0) \approx 0.37$ at the wall of $z = z_0$, or $\rho_w(z_0)$ (MC) $= 0.21$, which is less than the bulk density $\rho_0^* = 0.557$. Clearly, the adsorption is depletive.

Whilst, the contact values of the cavity functions $y_w(z_0)$ of the *naive* PY and HNC theories are at much higher values: being 1.6 and 1.8, respectively, as compared to 0.37 from MC. The (wall-particle) bridge function B_w (dotted line) from PY is shown in Figure (3.5), and is much subdued, being smaller (in magnitude) than the MC-inverted bridge function B_w (MC) (circles). This is symptomatic of the behaviour of many approximate closure equations derived from the uniform fluids. They are not applicable to the non-uniform case. The presence of the solid substrate exacerbates the inadequacies in the original PY and HNC equations. The new CA-OZ3-based closure is capable of curing this defect. We are able to show depletion effects and attain remarkable agreement with the MC data. Additional details about the benefit of the renormalization procedure can be observed if we compare the $\gamma_w(\vec{r})$ and $\gamma_H(\vec{r})$ as a function of the distance outside the wall, as shown for at $\rho^* = 0.557$ in Figure (3.6) (representative of all of

Figure 3.5: Inhomogeneous indirect correlation and bridge functions as a function of the distance from the wall for $\rho^* = 0.557$
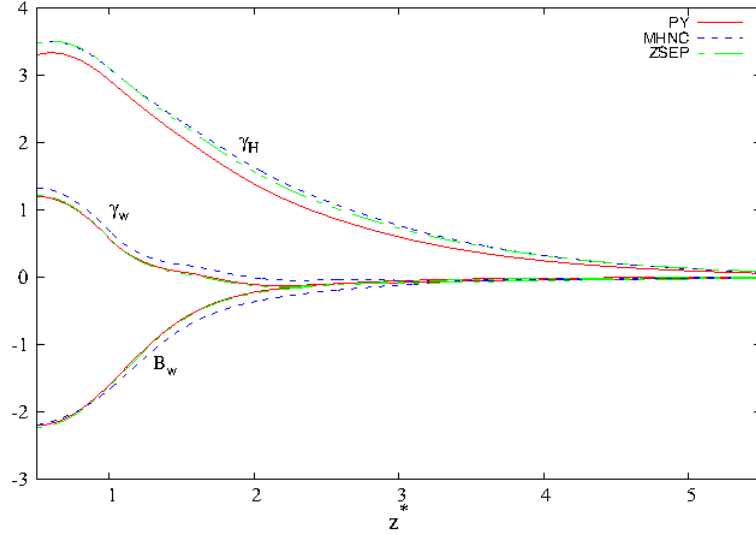
Figure 3.6: Duh-Haymet plots for $\rho^* = 0.557$
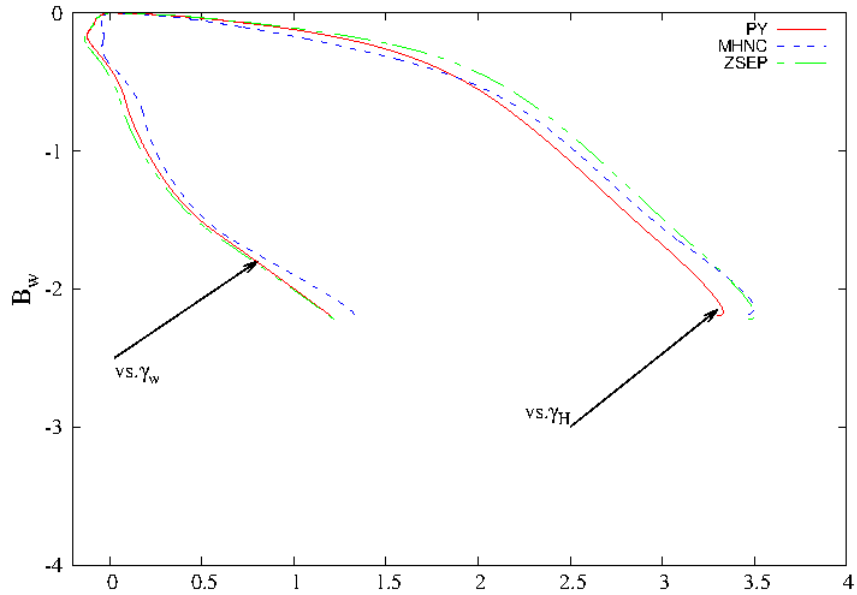
the densities considered). We notice that the renormalized $\gamma_H(\vec{r})$ are higher than the original $\gamma_w(\vec{r})$, owing to the core values $C_H^{(2)}(r)$ that enhance the functions values. $\gamma_H(\vec{r})$ is for most part positive and non-oscillatory. The importance of this treatment is easily revealed if we construct a so-called Duh-Haymet (DH) plot [109] for B_w vs. γ_H, as we compare it to the pair,

B_w vs. γ_w (see Figure (3.7)). While $B_w - \gamma_H$ is a well-behaved function, the un-renormalized $B_w - \gamma_w$ develops some kinks with multiple function values. These features come to show that B_w is a functional of γ_w and cannot be a simple function of γ_w. The relation is clearly not single-valued. From our perspective, these considerations highlight the importance of extracting out the extra-functional contributions in constructing the closure theory by implementing the re-normalization of γ_w, as is done here. The use of the base function γ_H is essential. It is of interest to compare the present OZ3-based theory with conventional DFTs based on the weighted-functions such as the FMT [103], and the non-uniform integral equation theory (e.g. the Lovett-Mou-Buff-Wertheim equation LMBW-1) [49]. Olivares-Rivas et al. [49] have reported the LMBW results, and Kim et al. [105] reported the FMT calculations for this Yukawa fluid at an HW. The λ range parameter they used was $\lambda = 1.8$. We examine two cases at temperatures $T = 1.25$ and 2.0. Both are at $\rho = 0.7$. In Figure (3.8), we report the comparison for $\rho = 0.7$ and $T = 2$. The MC data are available from Ref. [49]. The predictions of the CA-OZ3 theory with MHNC-$C_0^{(2)}$ input and FMT show comparable agreement with the MC profile of $y_w(z)$. The FMT is slightly superior in capturing the depth of the first minimum of $y_w(z)$. A slightly worse agreement is given by the CA-OZ3 based on the PY-$C_0^{(2)}$ input (solid line, Figure (3.8)) in reproducing the second peak, although the first minimum is well predicted. The LMBW-1 theory shows the worst agreement with the MC data, as it misses location and magnitude of the first valley. In Figure (3.9), we present the comparison for a more challenging thermodynamic state for the theoretical approaches, namely, the temperature is reduced to $T = 1.25$ (close to the critical temperature of the homogeneous hard-core attractive Yukawa fluid at $\lambda = 1.8$). At this temperature, the LMBW-1 theory (dotted line) is very poor, unable to capture the correct phase of the oscillations of the cavity function as the distance from the wall is increased. However, both versions (PY and MHNC $C_0^{(2)}$) of the CA-OZ3 theory reproduce the MC data quite accurately (see the full line and short dots, Figure (3.9)), and are shown to be even superior to the FMT approach, which overestimates the MC profile at reduced distance $r^* < 2$.

Closure:

$$B_w(\vec{r}) = -\frac{\zeta \gamma_H(\vec{r})^2}{2}\left[1 - \phi + \frac{\phi}{1 + \alpha \gamma_H}\right] + \psi \rho_0 \int dr' C_H^2\left(\mid \vec{r} - \vec{r'} \mid\right) \gamma_w\left(r'\right)\left[\gamma_w\left(r'\right) - h_w\left(r'\right)\right]$$

Table 3.1: The bulk pressure, $\frac{P_0}{kT}$ obtained from (i) an accurate integral equation for uniform fluids, i.e. MHNC, (ii) the MC contact density $\rho_w \left(z = \frac{\sigma}{2} \right)$, and (iii) the $\rho_w \left(z = \frac{\sigma}{2} \right)$ obtained from solving the EL equation with the new bridge function CA-OZ3.

		$T^* = 0.76$	
ρ^*	$\frac{P_0}{kT}$	$\rho_w \left(z = \frac{\sigma}{2} \right)$ (MC)	$\rho_w \left(z = \frac{\sigma}{2} \right)$ (CA-OZ3)
0.358	0.13	0.13	0.14
0.473	0.15	0.15	0.15
0.557	0.22	0.21	0.23

Note: The input uniform-fluid pair direct correlation functions $C_0^{(2)}$ are also calculated by the MHNC theory.

Figure 3.7: Inhomogeneous cavity functions as a function of the distance from the wall for $\lambda = 1.8$, $T = 2.0$, and $\rho = 0.7$
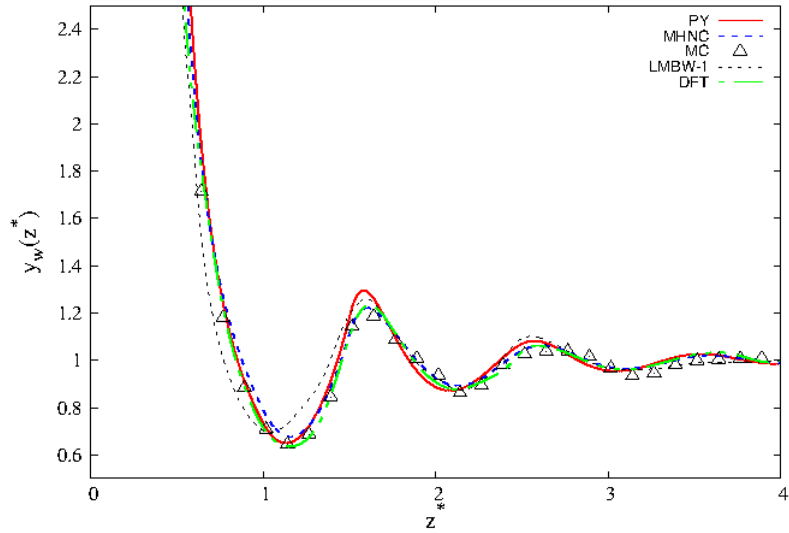
Table 3.2: Parameters used in the renormalized CA-OZ3 equation

$T^* = 0.76$								
ρ^*	α		ϕ		ζ		ψ	
	PY	MHNC	PY	MHNC	PY	MHNC	PY	MHNC
0.358	0.01	-0.35	0.50	1.50	0.85	0.28	6.0	6.0
0.473	0.20	0.20	2.50	2.50	0.90	0.80	0.9	0.9
0.557	0.25	0.21	1.74	2.39	0.40	0.60	0.25	0.25

$T^* = 1.25$								
ρ^*	α		ϕ		ζ		ψ	
	PY	MHNC	PY	MHNC	PY	MHNC	PY	MHNC
0.700	0.585	0.540	1.0	1.0365	1.0	1.066	0.0	0.0009

$T^* = 2.00$								
ρ^*	α		ϕ		ζ		ψ	
	PY	MHNC	PY	MHNC	PY	MHNC	PY	MHNC
0.700	1.70	1.00	1.20	1.20	1.50	1.70	0.001	0.0

Note: PY and MHNC refer to the corresponding homogeneous inputs for $C_0^{(2)}(r)$.

Figure 3.8: Inhomogeneous cavity functions as a function of the distance from the wall for $\lambda = 1.8$, $T = 1.25.0$, and $\rho = 0.7$

Figure 3.9: Inhomogeneous cavity functions and bridge function from nonuniform HNC and PY closures for $\rho = 0.557$
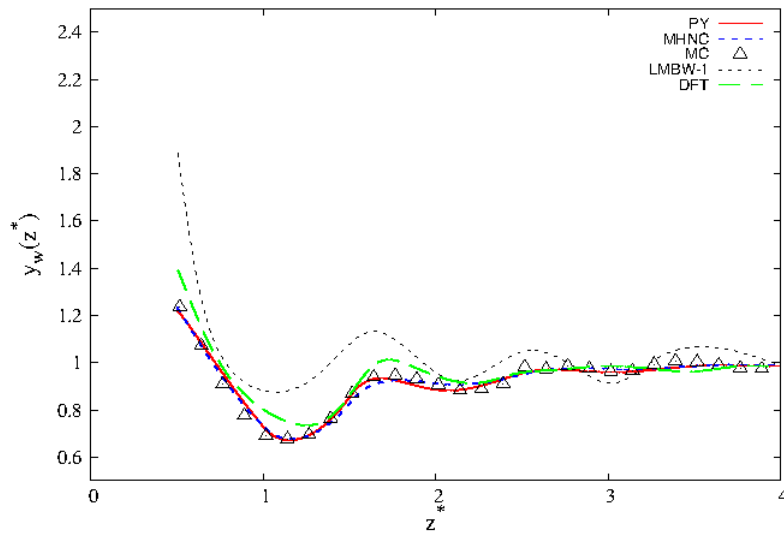
Chapter 4

Monte Carlo Computer Simulation of a binary hard-core Yukawa mixture

4.1 Introduction

Computer simulation is generically that approach where we make use of a computer to model and reproduce the behavior of a real system. We can distinguish among three different broad categories of computer simulation, according to the kind of usage we make of it: it can be used for heuristic purposes, to predict a data that is not known, and thirdly, when we model a system to understand some data that we already know. In physics, simulations are used wherever there is a governing theory that can guide the construction of a mathematical model. Equation-based simulations are very commonly used in the physical sciences, where the governing theory is most likely based on differential equations [110]. In statistical physics, that is the discipline whose framework we are working in, computer simulations can help us in predicting the value of thermodynamic quantities. In the following discussion, we will give for granted the knowledge of some statistical physical concepts, such as for instance the one of statistical *ensemble*.

When we consider computer simulations as applied to systems of particles interacting with some specific microscopic forces within statistical physics, there are two main types of approaches, namely Monte Carlo (MC) and Molecular Dynamics (MD). The specific way thermodynamic quantities are calculated within the two techniques is different: while MC simulations generate random walks in weighted regions of phase space to perform *ensemble* averages, in MD simulations time averages are calculated by numerically integrating the equations of motion of the system.

With the exception of the microcanonical ensemble, for which energy and total momentum are

constants of motion (Monte Carlo does not have a kinetic term), both MC and MD simulations are possible in a number of ensembles, including for example the canonical (constant temperature, NVT), isobaric (constant pressure, NPT). However, due to its peculiar nature, MC simulations can be performed in a much larger variety of ensembles, like for instance the grand canonical ensemble and the Gibbs ensemble. The discrepancy between the values of thermodynamic quantities as calculated within the two methods is usually small, and depending on the choice of the ensemble, these tiny differences are a result of the different magnitude of the associated mean-square fluctuations in finite-size systems.

In our study we considered a system of a constant number $N = N_A + N_B$ of identical particles belonging to two different species, at a fixed temperature ($\mathbf{T}$) and a fixed volume ($\mathbf{V}$). We used MC simulation to study the behaviour of this binary mixture in the NVT-ensemble. Before discussing the model of interaction between the particles of our system, we will describe in the next section some basic principles underlying the MC method.

4.2 *Ensemble* averages

In (classical) statistical mechanics, the expression of the partition function of a system consisting of particles belonging to the same chemical species (monocomponent system) is

$$Q = c \int d\mathbf{p}^N d\mathbf{r}^N exp \left[\frac{-H(\mathbf{r}^N, \mathbf{p}^N)}{k_B T} \right] \tag{4.1}$$

Where $\mathbf{r}^N$ and $\mathbf{p}^N$ are the coordinates of all N particles and their corresponding momenta, respectively, k_B is the Boltzmann constant and T is the absolute temperature. c is a constant of proportionality, chosen to approximate the sum $\sum_i exp(-E_i/k_B T)$ over quantum states to the classical partition function in the limit the Planck constant (divided π) $\hbar \rightarrow 0$. In equation (4.1) $H(\mathbf{r}^N, \mathbf{p}^N)$ is the total Hamiltonian of the system and it is expressed as $H = K + U$ where K is the kinetic energy and U is the potential energy. The statistical average of an observable A, expressed as a function of positions and momenta of the particles of the system, has the following expression

$$\langle A \rangle = \frac{\int d\mathbf{p}^N d\mathbf{r}^N A(\mathbf{r}^N, \mathbf{p}^N) exp[-\beta H(\mathbf{r}^N, \mathbf{p}^N)]}{\int d\mathbf{p}^N d\mathbf{r}^N exp[-\beta H(\mathbf{r}^N, \mathbf{p}^N)]} \tag{4.2}$$

where $\beta = 1/k_B T$. We can carry out the integration over momenta in the above equation analytically, since K is a quadratic function of the momenta. Because of this, we can easily evaluate averages of functions that depend on the momenta, the only part of the microscopic observables that gets difficult to evaluate are the one which depends on the particles' coordinates $A(\mathbf{r}^N)$. Since a multidimensional integral over particle coordinates can be computed only in a extremely restricted number of cases analytically, in most cases we have to use numerical techniques to compute it. If we want to solve the integral for the observable $\langle A \rangle$ above, the use of

standard numerical quadrature, such as for instance Simpson's rule, would be useless even if the number of independent coordinates $3N$ is very small. In fact, let us consider a mesh of points in the $3N$-dimensional configuration space, in which we will try and evaluate the integrand on. If we select m equidistant points on each coordinate axis, we then would have m^{3N} points at which we must evaluate our integrand. More unfortunately, since the Boltzmann factor in equation (4.2) is a function that varies rapidly according to the configuration of the system for most intermolecular potentials, we would need a small spacing mesh spacing for an accurate quadrature. Clearly we need better a numerical technique specifically suited to address the problem at hand: Monte Carlo importance sampling or the Metropolis Monte Carlo Method are a suitable solution of our problem.

4.3 Importance sampling and the Metropolis method

Metropolis *et al* realized that we can still evaluate the relative probability of two arbitrary configurations of the system even if we do not know the absolute probability density reported in equation (4.3) of finding the system in a configuration $\mathbf{r}^N$:

$$\mathcal{N}(\mathbf{r}^N) = \frac{exp[-\beta U(\mathbf{r})^N]}{Z}. \tag{4.3}$$

where Z in the above equation is the configurational part of the partition function Q:

$$Z = \int d\mathbf{r}^N exp[-\beta U(\mathbf{r})^N]. \tag{4.4}$$

This is possible since the relative probability is just given by the ratio of two absolute probability densities, i.e. the Boltzmann factor of the energy difference between the new configuration and an old one. Let us next consider how to generate particle configurations in the configuration space of the system (the Cartesian hyperspace with the $3N$ coordinates of the particles of the system) with a probability proportional to the Boltzmann factor. Let us denote the initial configuration $\mathbf{r}^N$ by the symbol o (old), and the associated Boltzmann factor as $exp[-\beta U(o)]$. The next step will then be to generate a trial configuration $\mathbf{r}'^N$ denoted by n (new) with a Boltzmann factor $exp[-\beta U(n)]$. The trial configuration can be achieved by allowing a very small but random displacement of a particle Δ. Now we need to decide whether to accept or to reject the trial configuration, and we can make this decision as based on the constraint that the probability of finding the system in the new configuration is proportional to $\mathcal{N}(n)$. This approach is known as the Metropolis method and we now discuss how it works. First of all, let us try to "*derive*" the transitional probability $(\pi(o \rightarrow n))$ in moving from an old configuration to a new one. We do this by means of a thought experiment. We are carrying out a large number (M) of MC simulations simultaneously, where our number M is much larger than the total number of accessible configurations. If m(o) is the total number of configurations o we had at the beginning,

then we want on average m(o) to be proportional to $\mathcal{N}(o)$. Obviously, once thermal equilibrium is reached, we want that the total number of moves from o to n be equal to the total number of reverse moves, which is the condition of **detailed balance**:

$$\mathcal{N}(o)\pi(o \rightarrow n) = \mathcal{N}(n)\pi(n \rightarrow o) \qquad (4.5)$$

where we indicated with π the so-called transition matrix. The latter is related to two steps: the first stage is when we perform a trial move from state o to n. The second stage is to decide whether to accept or reject this trial move. Let us call the probability of performing a trial move from o to n by $\alpha(o \rightarrow n)$, and the probability of accepting a trial move from o to n by $acc(o \rightarrow n)$. Then the transition probability ($\pi(o \rightarrow n)$) in moving from o to n is written as a conditional probability in terms of these two:

$$\pi(o \rightarrow n) = \alpha(o \rightarrow n) \times acc(o \rightarrow n). \qquad (4.6)$$

If we choose α to be a symmetric matrix, i.e. $\alpha(o \rightarrow n) = \alpha(n \rightarrow o)$, then equation (4.5) can be written as

$$\mathcal{N}(o) \times acc(o \rightarrow n) = \mathcal{N}(n) \times acc(n \rightarrow o), \qquad (4.7)$$

from which we get the ratio

$$\frac{acc(o \rightarrow n)}{acc(n \rightarrow o)} = \frac{\mathcal{N}(n)}{\mathcal{N}(o)} = exp\{-\beta[U(n) - U(o)]\}, \qquad (4.8)$$

which is a condition that can be satisfied by many choices of $acc(o \rightarrow n)$, provided the probability $acc(o \rightarrow n)$ is less or equal to 1. The simple recipe by Metropolis *et al.* was:

$$acc(o \rightarrow n) = \begin{cases} N(n)/N(o), & \text{if } N(n) < N(o). \\ 1, & \text{if } N(n) \geq N(o). \end{cases} \qquad (4.9)$$

The practical meaning of the formulas reported above is the following one: suppose we perform a trial displacement for a particle from state o to state n with $U(n) > U(o)$, this trial move should be accepted with a probability

$$acc(o \rightarrow n) = exp\{-\beta[U(n) - U(o)]\} < 1 \qquad (4.10)$$

The decision to whether accept or reject this trial move is based on the comparison of that probability with a random number Ranf generated uniformly within the interval $[0, 1]$. We accept the trial move if $\text{Ranf} < acc(o \rightarrow n)$, and we reject it if otherwise. However, if $acc(o \rightarrow n) > 1$ when the energy of the new state is lower than the energy of the old state, we accept the move unconditionally.

4.4 Some technicalities about a NVT Monte Carlo code

Most working Monte Carlo programs consist of a few hundreds to several thousand lines, and there is no standard Monte Carlo program though the cores of most MC programs look very similar. In summary, the core part of a MC code working in the NVT ensemble performs the following actions:

1. Random selection of a particle and calculation of the energy $U(o)$ of this particle with the surrounding ones.

2. Displacement of the particle along a random direction by a distance Δ, and calculation of the new energy $U(n)$

3. Choose whether or not to accept the move from the old configuration to the new with acceptance probability:

$$acc(o \rightarrow n) = exp[-\beta[U(n) - U(o)]] \tag{4.11}$$

A Monte Carlo program should be constructed such that it provides correct results without wasting computer time. A standard trick in building a computer simulation code is that of periodic boundary conditions (PBC), so to provide an homogeneous environment to all the particles of the system and simulate the so-called *bulk* conditions. In a few words, periodic boundary conditions replicate the simulation boxes along all the axes of symmetry. When considering like in our case a cubic box, the simulation cube is surrounded by similar cubes attached to all its faces so that a particle exiting the principal cube from one face enters the same cube from the opposite one. The issue that PBCs are meant to solve is that the number of particles one can manage to consider in a computer simulation is tens of orders of magnitude less than the typical number of molecules in a macroscopic sample. On typical, modern workstations, only a few hundreds to a few millions of particles can be used in a simulation, and the latter are at the reach of only the most powerful computers. Obviously, when considering a very small number of particles in a simulation, one must be very careful that the periodic boundary conditions do not affect the equilibrium properties of the system.

Let us briefly discuss how thermodynamic quantities can be calculated in finite simulation boxes by considering for example the configurational energy of a system of particles interacting via pairwise potentials $u(r_{ij})$, where r_{ij} is the distance between particles i and j. In general to calculate the total energy of the system in this virtually infinite system (because of PBCs), one would need to write it as an infinite sum of the terms. In practice, we particles interact via short-range forces. To allow for short range interactions only we introduce a cutoff distance r_c, so that any residual inter-particle interactions beyond this distance are set to zero. The potential energy contribution of a selected particle i is then provided by the interactions that are within the cutoff distance r_c from it. The error that may result from the truncation of these interactions

can be made arbitrary small by choosing r_c to be sufficiently large. If we take into account the presence of PBCs, it is easy to realize that the maximum value we can choose for r_c is equal to $L/2$ (half the box side) in order to prevent counting some of the interactions more than once (a given particle i could interact with a particle j and with its other nearest periodic image). The error in total molecular potential U^{tot} that might result from the truncation of the intermolecular interactions may be corrected by adding a tail contribution:

$$U^{tot} = \sum_{i<j} u_c(r_{ij}) + \frac{N\rho}{2} \int_{r_c}^{\infty} dr u(r) 4\pi r^2 \tag{4.12}$$

where u_c is the truncated potential energy function and ρ is the number density. There are also other ways to truncate the potential but we are not going through them in detail because we won't even use the tail corrections in our calculations: we will set r_c long enough that it will be negligible.

When setting up a system in the simulation box, all particles in it should be assigned an initial position. All reasonable initial conditions are acceptable (in the case of hard-core particles we should obviously avoid that particles overlap in the initial configuration) since the equilibrium properties of the system are expected not to depend on the initial state of the system. Once the system has reached equilibrium, quantities of interest can be calculate in cumulation runs starting a new simulation from the last configuration reached by the old run. run. When performing a simulation, it is always advisable to use quantities like temperature (T), density (ρ) and pressure (P) in reduced units. An important reason for using reduced units is that, even after changing the potential parameters many combinations of ρ, T, ϵ and σ will correspond to the same state in reduced units, which allow comparison of results. Reduced units are by definition dimensionless. For example, for a monocomponent system the reduced pressure (P^*), reduced density (ρ^*), and the reduced temperature (T^*) have the following expressions: $P^* = P\sigma^3\epsilon^{-1}$, $\rho^* = \rho\sigma^3$, $T^* = k_B T\epsilon^{-1}$.

4.5 Acceptance probabilities for a binary mixture in the NVT ensemble

For a binary mixture containing particles of species A and species B, we have $N = N_A + N_B$ particles distributed over the volume V. We define scaled coordinates $\mathbf{s}_k^N = \frac{\mathbf{r}_k^N}{V_k^N}$, where $k = 1, 2$. It follows from Eq. (4.1) that the partition function for a binary mixture with fixed volume V is given by:

$$Q_G(V, N_A, N_B, T) = \frac{1}{\Lambda^{3(N_A+N_B)}N_A!N_B!} \int \mathbf{s}^{N_A}\mathbf{s}^{N_B} exp[-\beta(U_A(\mathbf{s}^{N_A}) + U_B(\mathbf{s}^{N_B}) + U_{AB}(\mathbf{s}^{N_A}, \mathbf{s}^{N_B}))],$$

$$\tag{4.13}$$

where Λ is the thermal deBroglie wavelength. From this we can establish that the probability density is given by

$$\mathcal{N}(N_A, N_B, V, T) \propto exp[-\beta(U_A(\mathbf{s}^{N_A}) + U_B(\mathbf{s}^{N_B}) + U_{AB}(\mathbf{s}^{N_A}, \mathbf{s}^{N_B}))], \qquad (4.14)$$

We need to develop acceptance rules for the displacement moves of each species separately. Consider the situation in which a state n is obtained when a state o experiences a displacement of a particle of species A in box 1. It follows from Eq. (4.14) that the ratio of the probability densities of the two states is:

$$\frac{\mathcal{N}(n)}{\mathcal{N}(o)} = \frac{exp[-\beta[U_A(\mathbf{s}_n^{n_A}) + U_{AB}(\mathbf{s}_n^{n_A}, \mathbf{s}_n^{n_B})]]}{exp[-\beta[U_A(\mathbf{s}_o^{n_A}) + U_{AB}(\mathbf{s}_o^{n_A}, \mathbf{s}_o^{n_B})]]}, \qquad (4.15)$$

giving us the following acceptance rule according to the Metropolis sampling for when a particle of species A is displaced within the simulation box:

$$acc(o \to n) = min(1, exp[-\beta[U_A(\mathbf{s}_n^{n_A}) + U_{AB}(\mathbf{s}_n^{n_A}, \mathbf{s}_n^{n_B}) - U_A(\mathbf{s}_o^{n_A}) - U_{AB}(\mathbf{s}_o^{n_A}, \mathbf{s}_o^{n_B})]]). \quad (4.16)$$

Suppose now we consider the case in which a particle of species B is displaced in the simulation box such that the configuration of the system changes from a state o to a new state n. Applying the same procedure to calculate the ratio of the probability densities for the case when a particle of species B is displaced yields the acceptance rule:

$$acc(o \to n) = min(1, exp[-\beta[U_B(\mathbf{s}_n^{n_B}) + U_{AB}(\mathbf{s}_n^{n_A}, \mathbf{s}_n^{n_B}) - U_B(\mathbf{s}_o^{n_B}) - U_{AB}(\mathbf{s}_o^{n_A}, \mathbf{s}_o^{n_B})]]). \quad (4.17)$$

4.6 Model and Method

In our study we considered a binary mixture of hard-core Yukawa (HCY) particles having the same diameter $\sigma_{AA} = \sigma_{BB}$ for different system sizes $N = 108, 256, 512, 1026, 1876$, where N is the total number of particles belonging to both A and B species. Then $N = N_A + N_B$, and we fixed $N_A = N_B$ (equimolar mixture) throughout our calculations. The two-body potential for the hard-core Yukawa particles is given by

$$u_{ij}(r) = \begin{cases} \infty, & \text{if r} < \sigma_{ij} \\ -\frac{\epsilon_{ij}\sigma_{ij}exp[-\lambda(r-\sigma_{ij})]}{r}, & \text{if r} \geqslant \sigma_{ij} \end{cases} \qquad (4.18)$$

where σ_{ij}, ϵ_{ij}, and λ are, respectively, the collision diameter and the energy parameter between particles belonging to species i and j, $\lambda = 2.45\sigma_{AA}^{-1}$ is the inverse decay parameter, and r is the center-to-center distance between two interacting HCY particles. The crossed collision diameter

$\sigma_{AB} = (\frac{(\sigma_{AA}+\sigma_{BB})}{2})(1 + \Delta)$ is written in terms of the nonadditive parameter Δ. When Δ assumes negative values particles belonging to different species can approach each other to a distance lower than the arithmetic average of their diameters, while the distance of minimum approach is enhanced beyond that value when Δ assumes positive values. Here we considered systems with $\Delta = 0, \pm 0.1$. In all our calculations, we set $\epsilon_{BB} = 2\epsilon_{AA}$ and we varied the crossed energy parameter in the interval between $\epsilon_{AB} = 1.2\epsilon_{AA}$ and $2\epsilon_{AA}$. We used σ_{AA} and ϵ_{AA} as units of measure for lengths and energies, respectively. We fixed the reduced temperature $T^* = k_B T/\epsilon_{AA}$ of the system to $T^* = 1$, and the reduced density $\rho^* = N/V\sigma_{AA}^3$ to $\rho^* = 0.75$.

We performed NVT Monte Carlo simulations of the HCY binary mixture. Initial configurations were generated by putting an initial, equal number of particles of the two species in the simulation box with cubic periodic boundary conditions. Subsequently, an attempt was performed to displace all the particles, while at the same time the cavities generated in correspondence of the sites of a cubic grid with a tiny mesh were monitored. Particles were added to these cavities and if no cavities were detected we continued displacing particles randomly until a cavity was detected. We iterated this procedure until the desired density was reached. During this procedure, particles were randomly displaced inside the box and we only took care that they did not overlap with each other, depending on the values chosen for their diameters. After generating an initial configuration of particles in the box, we performed not less than 10^5 MC cycles to equilibrate the system. A MC cycle consists in a number of attempts to displace randomly selected particles inside the simulation box, that was set equal to the total number of particles. The direction of displacement was also randomly selected, and we managed to obtain an acceptance rate for particle displacements of the two species equal to 50%. Following equilibration, we performed a cumulation run of 5 blocks of 2×10^5 MC cycles to calculate the averages of the thermodynamic quantities and the radial distribution functions (rdfs) g_{ij}, where $i, j \equiv A, B$. Rdfs were also used to calculate the pressure P of the system, according to the well-known statistical-mechanical identity for hard-core particles interacting with a soft potential:

$$\frac{\beta P}{\rho} = 1 + \frac{2}{3}\pi\rho \sum_i \sum_j c_i c_j [\sigma_{ij}^3 g_{ij}(r) - \beta \int_{\sigma_{ij}}^{\infty} v_{ij}'(r)g_{ij}(r)r^3 dr]. \qquad (4.19)$$

We mainly use the virial equation in order to calculate the pressure of the system. In this identity, we do not need to perform any numerical integration to get the contribution of the pressure coming from the soft part of the pair potential, like in Eq. 4.19. The formula for the virial equation is reported in standard textbooks for a monocomponent system. We originally extended it to binary mixtures of two species A and B in the Appendix of this thesis since we could not find its expression in any article reported in the scientific literature, even though people might have used it and have just considered its extension to binary mixtures as a trivial task. The quantity $\frac{\beta P}{\rho}$ also takes the name of *compressibility factor*, and it is expected to become equal to 1 for an ideal gas.

4.7   Results and Discussion

The model and the model parameters that we targeted were already investigated in the literature in References [9] and [87]. The model parameters were chosen so that one of the two species possesses an enhanced self-energy, i.e. the energy parameter for BB interactions is twice as much as the one of AA interactions, while the diameter of the two species is the same. The higher energy parameter for BB interactions then favours self-interactions among B particles, thus making the possibility of the system to phase separate into two distinct phases in composition (where one of the two phase is more dense in B particles) very likely. When we look at the total configurational energy per particle of the system for different values of the crossed energy parameter ϵ_{AB}, we expect a non-monotonic behaviour especially when the ratio $\frac{\epsilon_{AB}}{\epsilon_{BB}}$ becomes considerably less than 1. In fact, provided the energy parameter between the two different species is comparable with the one for the interactions between B particles, we expect that the tendency of the system to segregate should be compensated by the tendency of particles belonging to different species to mix up with each other. However, when that is not the case anymore the system might experience a phase transition, or might be forming equilibrium clusters of B particles, as it is discussed above. In one of the latter cases, we expect that even the total configuration energy of the system would show a remnant of this microscopic rearrangement of the system. However, if we look at the symbols of Figure 4.1, which are related to the MD energies reported in the literature for a system of 108 particles, we easily realize that the increasing the crossed energy parameter from $\epsilon_{AB} = 1.2$ (bottom symbol) up to $\epsilon_{AB} = 2$ (top symbol) is reflected into a monotonic decrease of the configurational energy of the system (we reported minus one times the configuration energy in the Figure). A system of 108 particles, also considering that we are focusing on a binary mixture, appears as a very small-sized one. The authors of Ref. [9] also mention that they have checked for the absence of finite-size effects on systems of 256 particles but do not provide any details about that comparison. When considering systems of such small size, the periodic boundary conditions play a non-trivial role and especially if the system is in a two-phase region, the interfacial energy separating the two phases is a huge component of the total energy, thus considerably biasing the thermodynamic equilibrium of the system. More unfortunately, in Ref. [9] the details about the duration of the simulations, e.g. the duration of the equilibration runs before getting the average thermodynamic properties of the system in cumulation runs, makes us worry whether the system was equilibrated for long enough. This state of affairs prompted us to perform a finite-size study of the dependency of the energy per particle on the size N of the system, that is also reported in Fig. 4.1 for the different values of ϵ_{AB}. The picture emerging from our calculations upholds the concern about the inadequacy of the small size reported in the literature for the system under study. In fact, we note that for all the considered values of ϵ_{AB} the energy per particle becomes nearly insensitive to the size of the system only for sizes exceeding $N = 1000$ (the lines which are reported in the Figure to guide the
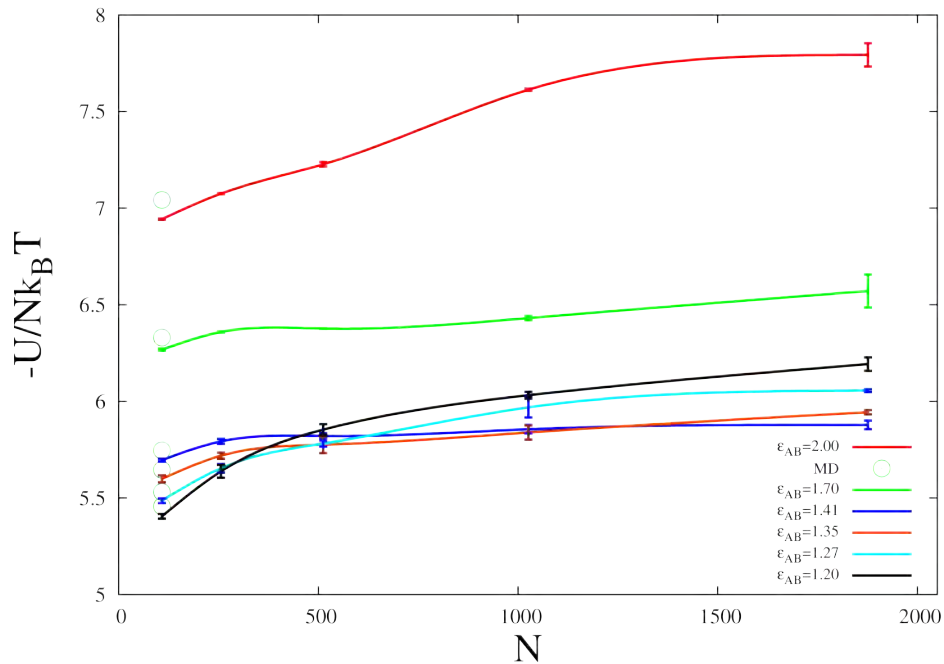
Figure 4.1: Configurational energy per particle for the HCYM for different values of ϵ_{AB} (see legend) as a function of system size (total number of particles in the box) at $T^* = 1.0$ and $\rho^* = 0.75$. Error bars are our MC results. Lines are a guide for the eye. Symbols are the MD results reported in [9] and they are piled up in ascending order starting from $\epsilon_{AB} = 1.2$ (bottom symbol) to $\epsilon_{AB} = 2$ (top symbol).

eye become nearly flat). Our estimates at $N = 108$ are slightly different than the MD ones, and this is not surprising considering the different computer simulation methodology adopted and also the small time-frame that was adopted by the authors of Ref. [9] to equilibrate the system during the MD runs. Our results for such small system size are consistent with the ones reported in [9], and confirm that the total energy per particle monotonically decreases with the increase of the parameter ϵ_{AB}. However, when we consider the more reliable system sizes the picture is completely different for small values of ϵ_{AB}: we observe that the energy per particle decreases when the parameter ϵ_{AB} increases up to $\epsilon_{AB} = 1.41$. The magnitude of this energy depletion diminishes as we increase ϵ_{AB} up to $\epsilon_{AB} = 1.41$. Then, the monotonic increase with ϵ_{AB} takes over again. The explanation that we can sketch for the moment is that for small values of ϵ_{AB} in comparison to $\epsilon_{BB} = 2$, this behaviour could be compatible with a loss of the energy per particle of the system when we increase the value of the crossed energy parameter. In fact, B particles are going to be subtracted from the B-rich environment which they tend to form in the simulation box when we make the crossed interaction between species more appealing (by increasing the value of the crossed-interaction energy parameter). Another feature that could indicate that for the smallest value of $\epsilon_{AB} = 1.2$ considered, the system might be in a two-phase region is the fact

we did not reach a situation where the energy per particle becomes insensitive to N (see the black line reported in Fig. 4.1). In this case, the formation of an interface or multiple interfaces between the two phases at different composition inside the simulation box could represent a problem; in fact, it would introduce an energetic bias making the energy per particle dependent on the system size since the number of particles exposed to the interface will grow accordingly. This situation makes the choice to equilibrate the system by discarding the first 6000 configurations only after the particles were initially allocated to the sites of a FCC lattice in the MD simulations of Ref. [9], a very ill-made one, since the system would probably need more time to equilibrate properly. Besides this aspect, we also need to consider that MD simulations of discontinuous potentials (such as the HCYM) are generally statistically less accurate because of the technical difficulty to properly sample particle collisions [111].
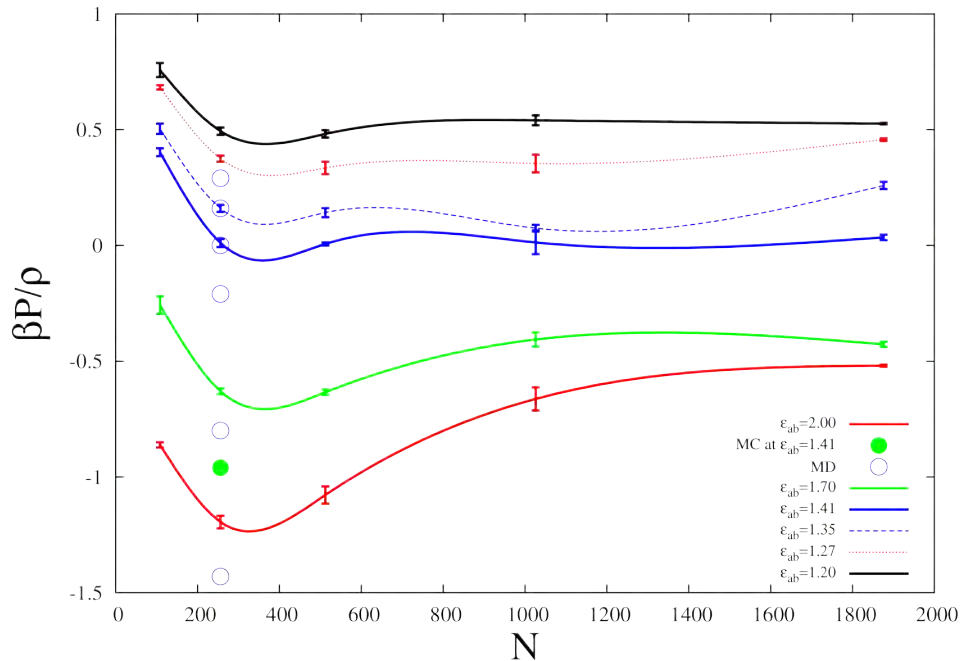

Figure 4.2: Compressibility factor for the HCYM for different values of ϵ_{AB} (see legend) as a function of system size (total number of particles in the box) at $T^* = 1.0$ and $\rho^* = 0.75$. Error bars are our MC results. Lines are a guide for the eye. Open circles are the MD results reported in [9] and they are piled up in ascending order starting from $\epsilon_{AB} = 1.2$ (bottom symbol) to $\epsilon_{AB} = 2$ (top symbol). The filled circle is the MC result reported in [112].

The same finite-size effect is shown in Fig. 4.2 for the compressibility factor, that is reported as a function of the system size N for the different values of ϵ_{AB} we considered. The discrepancy between our values of $\beta P / \rho$ for the smaller sizes and the MD ones reported in Ref. [9] are even more marked. Understanding the origin of this discrepancy is difficult since as we noted before the authors of Ref. [9] do not provide many technical details about their MD simulations, and

they even do not indicate clearly if their simulations were conducted for the system size $N = 108$ or $N = 256$ (we chose to put their results at the value $N = 256$ in Fig. 4.2). To better understand the wide range of variability of the estimates of $\beta P/\rho$, we also reported in Fig. 4.2 the only MC simulation data available in literature as reported in Ref. [112] for $N = 108$ and $\epsilon_{AB} = 1.41$ (filled circle in Fig. 4.2). If we compare this result with the one obtained in Ref. [9] (third open circle from the bottom), we easily realize the large discrepancy of the values of this quantity for small sizes even for data already published in the scientific literature. Another explanation different than the one related to the adequacy of the equilibration time chosen in the literature for MD simulations, could also be related to the kind of approach used to estimate the pressure since as we stated in the previous section there are essentially two different procedures (one based on the virial equation and the other one on the radial distribution functions (rdfs)), as well as a bias that could be introduced by the statistical accuracy with which rdfs are being calculated. In fact, the accuracy of the rdfs is going to affect both the hard-core and the soft contributions to the pressure (see equations for the pressure as reported in the previous section and in the Appendix). Finally, in Ref. [9] the usage of tail corrections having been applied to the estimate of the compressibility is mentioned, which we did not apply at the end of our simulations because we were more interested in the results provided by the higher system sizes. We also checked that our estimates performed in terms of the virial equation (see Appendix) and the rdf route were similar, and the two values are reported in Table 4.2.

In Fig.s 4.3 and 4.4, we report the energy per particle and the compressibility factor as a function of the crossed energy parameter ϵ_{AB}, respectively. In the Figures we compare our MC results for the biggest system size considered with the MD results reported in [9]. Both the two methods predict a monotonic decrease of the compressibility factor when the crossed energy parameter is increased, even if the values reported in the literature are very different ones and the reason is ascribable to the small system size considered in Ref. [9], as we have thoroughly discussed before. However, the effect of the finite-size effects is better illustrated by looking at Fig. 4.3, where the energy per particle as calculated by us exhibits a minimum as a function of ϵ_{AB}, while the MD simulations of Ref. [9] report an unlikely monotonic decrease (we remind that we reported the opposite of the energy per particle in the Figure) when the crossed energy parameter is increased.

The energy behaviour we observed before is better understood if we look at the rdfs of the system, which are reported in Figures 4.5 - 4.7 for the AA, AB, and BB correlations. The rdf provides us with the information of the probability of finding particles of the selected species at different distances from a generic target particle of the system. In these Figures, we compare the rdfs as calculated for a system size as the one considered in Ref. [9] with the biggest one we considered ($N = 1876$ particles). The very important indication we get in this case is related to the tendency of the truly representative system with the higher number of particles to phase-separate for small values of ϵ_{AB}. This feature is evident in the way the rdf profiles
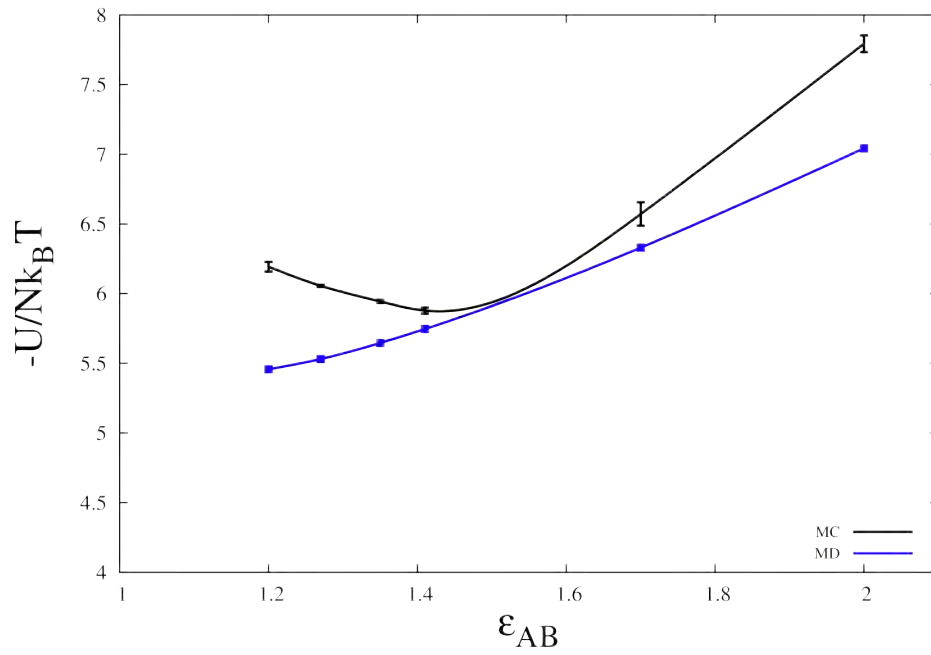
Figure 4.3: Configurational energy per particle for the HCYM as a function of ϵ_{AB} at $T^* = 1.0$ and $\rho^* = 0.75$. Error bars are our MC results for the biggest system size considered. Symbols are the MD results reported in [9]. Lines are a guide for the eye.

Figure 4.4: Compressibility factor for the HCYM as a function of ϵ_{AB} at $T^* = 1.0$ and $\rho^* = 0.75$. Error bars are our MC results for the biggest system size considered. Symbols are the MD results reported in [9]. Lines are a guide for the eye.
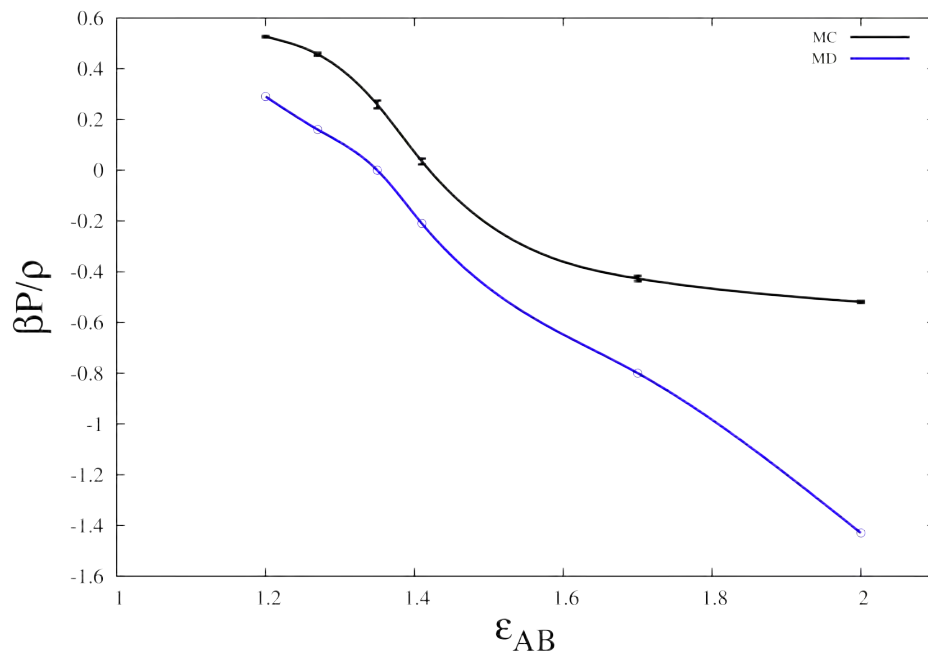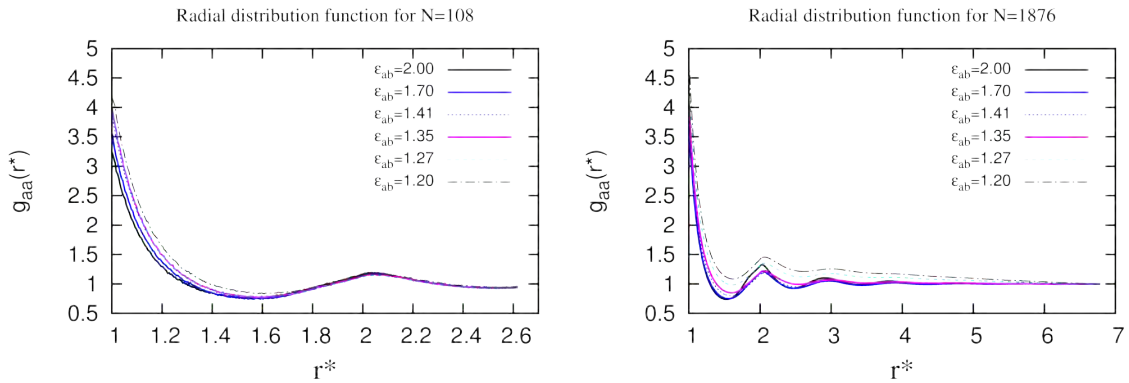
Figure 4.5: MC Radial distribution functions for $A - A$ particles as a function of distance at $T^* = 1.0$ and $\rho^* = 0.75$. Left panel: $N = 108$. Right panel: $N = 1876$.

approach the asymptotic limit of 1 for long distances: a fluid-like structural behaviour for the rdfs is associated with smooth oscillations of its profile around 1, which are related to particle correlations and to the formation of a shell-like structure around a generic particle of the fluid. These oscillations tend to damp out for higher distances when the rdf approaches its asymptotic limit of 1. However, in our case both the AA and the BB rdfs exhibit a clear trend to be well above 1 for the extended range of distances, when we consider the small values of ϵ_{AB}. This behaviour is typically associated with a tendency of the system to segregate into two A-rich and B-rich phases, and it is confirmed by the fact that the crossed AB rdf for the particles belonging to different species is consistently depleted below 1 over the same range of distances (see Fig. 4.6). If we zoom over short-distances very close to the contact value of $\sigma_{AA} = \sigma_{AB} = \sigma_{BB} = 1$ (see Figures 4.8-4.10, we can provide some better insight over the observed finite-size effect observed for the energy per bead of systems with small size.

In fact, while the AA and BB rdfs tend to be monotonically depleted as ϵ_{AB} increases for the system of larger size (see right panels of Fig.s 4.8,4.10), this effect does not hold for the systems of small size (see left panels of the same Figures). In fact, increasing the crossed energy parameter from $\epsilon_{AB} = 1.27$ to 1.35 does not bring the expected depletion of the AA and BB rdfs,

which stay pretty much the same, if they do not become even higher. The same behaviour is observed for the AB rdf: instead of becoming more enhanced from $\epsilon_{AB} = 1.27$ to 1.35, it remains almost unaltered. These results strongly suggest that the interfacial energy barrier separating the two A-rich and B-rich phases (or in absence of any free-energy calculations which would allow us to ascertain whether we are in a two-phase region or not, it is probably better to discuss about A-rich and B-rich local structures in the binary mixture) prevents
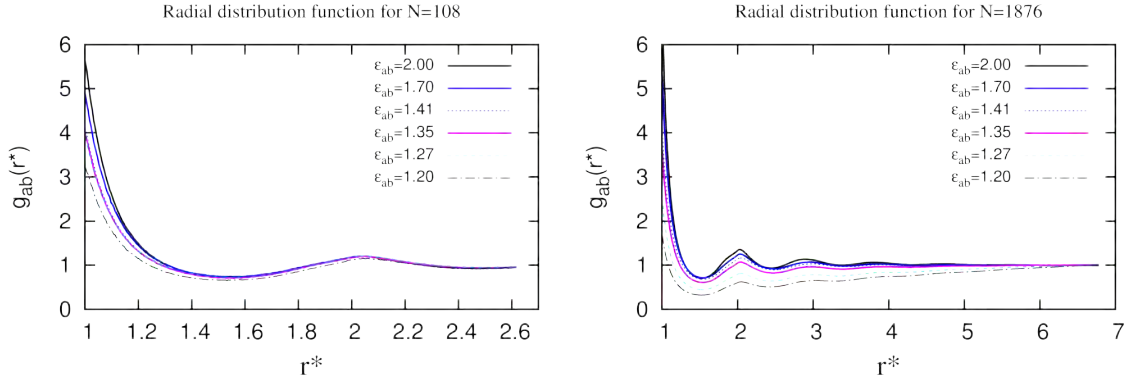

Figure 4.6: MC Radial distribution functions for $A - B$ particles as a function of distance at $T^* = 1.0$ and $\rho^* = 0.75$. Left panel: $N = 108$. Right panel: $N = 1876$.

the mixing up of the two species as driven by the increase of the parameter ϵ_{AB}. This drawback happens for small system sizes because it is exactly in these cases that a non-trivial contribution to the energy of the system comes from the particles at the interface between the two phases (or at the boundaries between the two A-rich and B-rich local structures). In summary, the small size of the system for a model where BB interactions are favoured ($\epsilon_{BB} = 2$) introduces a bias in the microscopic arrangement of the system, that is reflected into a wrong monotonic increase of the energy per particle when the crossed energy parameter ϵ_{AB} is increased. Obviously, this effect happens only when ϵ_{AB} is considerable less than ϵ_{BB}: when its value approaches ϵ_{BB} the energy is expected to monotonically increase as a function of ϵ_{AB}, as it is also clearly shown in our calculations.

Figure 4.7: MC Radial distribution functions for $B - B$ particles as a function of distance at $T^* = 1.0$ and $\rho^* = 0.75$. Left panel: $N = 108$. Right panel: $N = 1876$.

The last comparison we performed is with the data reported in Ref. [87], where the same system is investigated by allowing the nonadditive parameter Δ to assume values different than zero. In that paper, both positive and negative values of the nonadditive parameter were considered, which have the two opposite effects of favouring (negative) and unfavouring (positive) interaction between particles belonging to different species. We chose the extreme values of $\Delta = -0.1, 0.1$ in order to perform our calculations and compare them with those reported in Ref. [87]. The comparison for the energy per particle is still done by changing the value of the crossed energy parameter ϵ_{AB}, and it is reported in Table 4.1. Not surprisingly our results now reported for the biggest system size only ($N = 1876$), are very different than the ones obtained in Ref. [87], which were obtained again by performing MD simulations with a small system size of $N = 108$ particles. We are not focusing on criticizing the results reported in the literature because we are well aware at this point of the issues that simulating our system with a small number of particles may cause to the value of the thermodynamic quantities. On the contrary, we prefer to highlight the consistency of the neat and stimulating physical picture emerging from our data.

Let us begin our discussion of the results by comparing the values of the energy per particle for the negative value of Δ (-0.1) with the additive case ($\Delta = 0$). Let us consider first the extreme
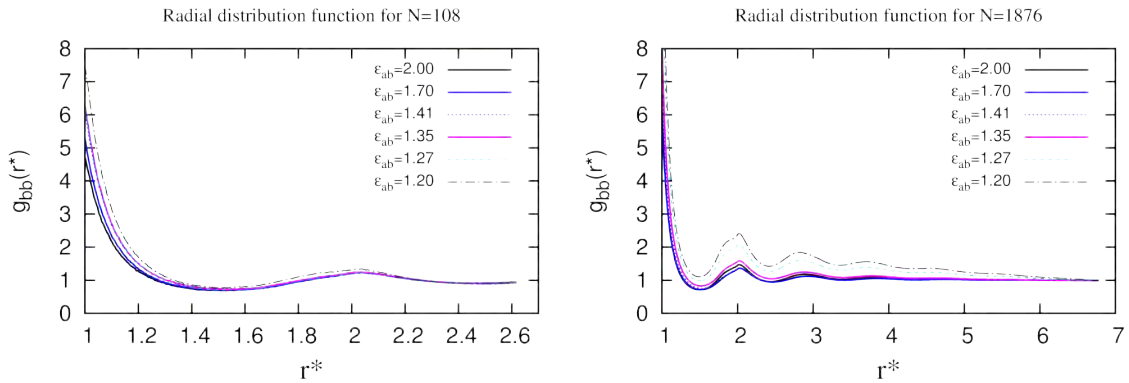
Figure 4.8: MC Radial distribution functions for $A - A$ particles as a function of distance at $T^* = 1.0$ and $\rho^* = 0.75$. Left panel: $N = 108$. Right panel: $N = 1876$. Rdfs are reported close to the contact values.

case of the lowest value of $\epsilon_{AB} = 1.2$. In this case, we observe that the value of U/Nk_BT is slightly higher than its counterpart at $\Delta = 0$. When the crossed energy parameter is sufficiently low as compared to $\epsilon_{BB} = 2$, we expect as before that the ability of A particles to interact with B particles will be significantly lowered. However, since Δ has a negative value the A particles can get closer to B particles than B particles themselves. Thus, by favouring AB interactions with a negative value of Δ we are depleting the total energy per bead as compared to the case $\Delta = 0$ with a small statistical number of A particles which can get closer to B particles, and provide a comparably much smaller energy contribution ($\epsilon_{AB} = 1.2$). However, when the parameter ϵ_{AB} increases we quickly observe that this effect does not hold true anymore, and now the energy per particle of the system with negative Δ becomes lower than in the additive case. The deviation between the two values becomes larger and larger when ϵ_{AB} is further increased until it achieves its final considered value $\epsilon_{AB} = 2$. The explanation of this effect is a very straightforward one: when the statistical number of A particles surrounding B particles goes up triggered by the increase of ϵ_{AB}, their energy contribution is still lower than the one offered by B particles but the negative value of Δ allows A particles to better pack around B ones. Thus, their likely higher
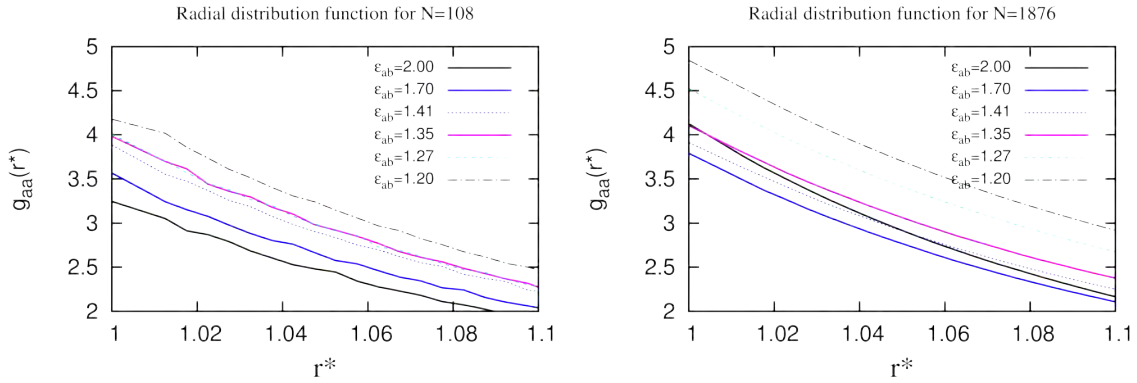
Figure 4.9: MC Radial distribution functions for $A - B$ particles as a function of distance at $T^* = 1.0$ and $\rho^* = 0.75$. Left panel: $N = 108$. Right panel: $N = 1876$. Rdfs are reported close to the contact values.

number than in the additive case provides the total energy per particle with an additional energetic contribution that makes the total energy per particle for $\Delta = -0.1$ lower than the case $\Delta = 0$. Obviously, this effect originates from a subtle competition between the energy loss determined by having less B particles surrounding B particles, and the energy gain provided by the exact energy contribution ϵ_{AB} of A particles when they get close to B particles. Our results demonstrate that in the range of ϵ_{AB} values being explored, the energy contribution originating by the higher statistical number of A particles surrounding B particles is of sufficient magnitude to even make the observed energy minimum as a function of ϵ_{AB} for the additive case to disappear.

When we consider the case of the positive value of the nonadditive parameter $\Delta = 0.1$, a different although not less interesting physical picture emerges if we compare the data against the case $\Delta = 0$ again. This time AB closer approaches are forbidden, and the way this feature is going to affect the total energy per particle is clearly reported in Table 4.1. For small up to intermediate values of ϵ_{AB} we observe that U/Nk_BT values for the nonadditive case are lower than the ones for the additive case. If the crossed energy parameter has not a value comparable to the one of
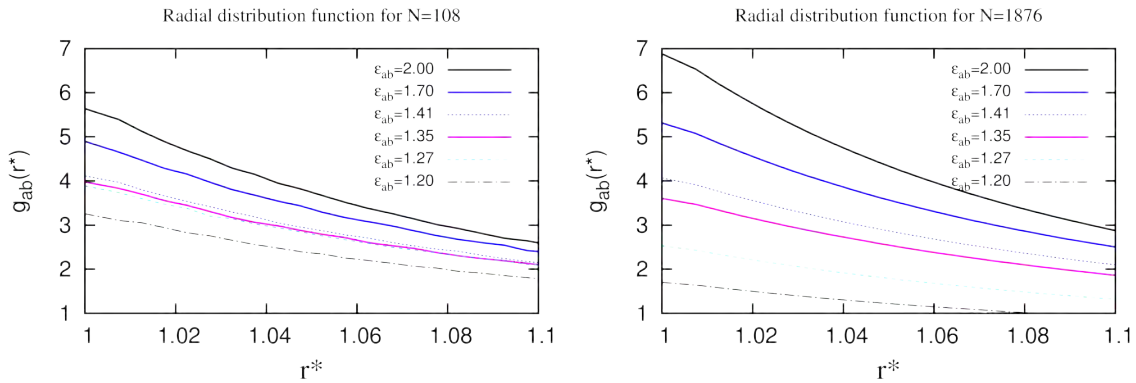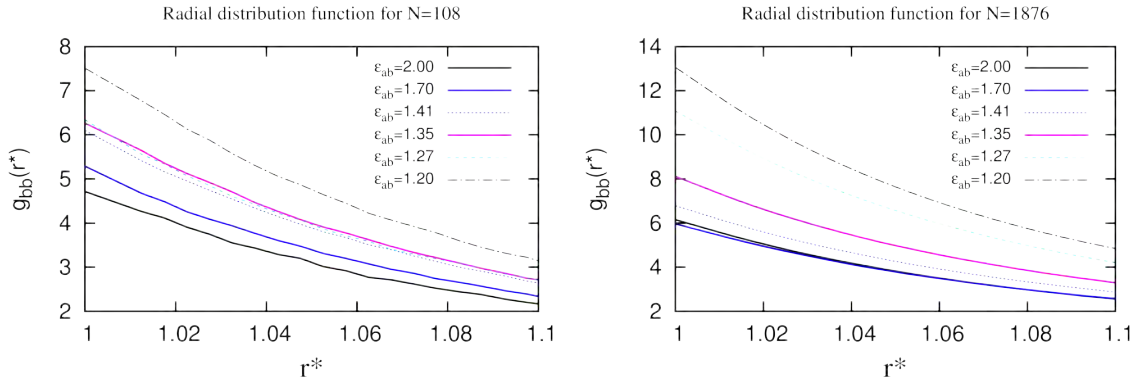
Figure 4.10: MC Radial distribution functions for $B - B$ particles as a function of distance at $T^* = 1.0$ and $\rho^* = 0.75$. Left panel: $N = 108$. Right panel: $N = 1876$. Rdfs are reported close to the contact values.

BB interactions $\epsilon_{BB} = 2$, since A particles are constrained to be at a larger distance from B particles by the positive value of Δ, their energy contribution to the total energy per particle will become depleted as compared to the additive case. It is interesting to note that this depletion is similarly as in the case $\Delta = -0.1$ in competition with the energy gain due to the statistical population of B particles surrounding a generic B particle which tends to shrink as ϵ_{AB} is increased. The effect of this competition eliminates again the minimum of U/Nk_BT as a function of ϵ_{AB} that was observed in the additive case, and we see that the energy per particle at $\Delta = 0.1$ is monotonically increasing as a function of the crossed energy parameter. Eventually, when $\epsilon_{AB} = \epsilon_{BB} = 2$, U/Nk_BT for $\Delta = 0.1$ becomes higher than the corresponding value at $\Delta = 0$. When the two energy parameters for BB and AB interactions get the same value, the larger distances that the population of A particles surrounding a B particle assumes, can explain the energy loss in comparison to the additive case. In fact, in this case the expected magnitude of the statistical population of A particles surrounding a B particle should be similar to the one of B particles surrounding a generic B particle.

For the sake of completion, we also report the pressures as estimated for the two considered,

nonadditive cases in Table 4.3.

Table 4.1: Monte Carlo (MC) values (the values in the brackets are the errors on the last digits) for the energy per particle $-U/Nk_BT$ for the HCYM at $\frac{k_BT}{\epsilon_{AA}} = 1$ and $\rho\sigma^3 = 0.75$. Different values of ϵ_{AB} and nonadditive parameters (Δ) are considered and the results are compared with previously published results obtained by Molecular Dynamics (MD).

<div align="center">

$-U/NK_BT$

ϵ_{AB}	MC (N=1876) ($\Delta = 0.0$)	MD ($\Delta = 0.0$)	MC (N=1876) ($\Delta = -0.1$)	MD ($\Delta = -0.1$)	MC (N=1876) ($\Delta = 0.1$)	MD ($\Delta = 0.1$)
2.00	7.793(60)	7.023	9.430(12)	6.549	7.523(9)	8.029
1.70	6.571(85)	6.327	8.001(6)	5.758	6.808(20)	7.231
1.41	5.878(22)	5.762	6.713(13)	5.217	6.546(16)	6.483
1.35	5.944(11)	5.664	6.488(18)	5.137	6.526(23)	6.356
1.27	6.056(8)	5.495	6.269(15)	4.998	6.491(31)	6.234
1.20	6.193(35)	5.381	6.052(22)	4.917	6.468(29)	6.136

</div>

Table 4.2: Same as in Table 4.1 for the compressibility factor from the virial equation (vir) and from the rdf route (rad), calculated using MC simulation of a system of 1876 particles at $\Delta = 0.0$

<div align="center">

$\frac{\beta P}{\rho}$

ϵ_{AB}	MC (vir) (N=1879) ($\Delta = 0.0$)	MC (rad) (N=1879) ($\Delta = 0.0$)	MD
2.00	-0.5192 ± 0.0044	-0.6350 ± 0.0041	-1.43
1.70	-0.4269 ± 0.0111	-0.5120 ± 0.0109	-0.80
1.41	0.0347 ± 0.0116	-0.0377 ± 0.0113	-0.21
1.35	0.2587 ± 0.0156	0.1817 ± 0.0148	0.00
1.27	0.4568 ± 0.0060	0.3727 ± 0.0063	0.16
1.20	0.5260 ± 0.0028	0.4371 ± 0.0031	0.29

</div>

Table 4.3: Same as in Table 4.2 but for the reduced pressure $\frac{\beta P_{vir}}{\rho}$ calculated from the virial equation at $\Delta = \pm 0.1$.

| | $\frac{\beta P_{vir}}{\rho}$ | |
ϵ_{AB}	MC (N=1879) ($\Delta = -0.1$)	MC (N=1879) ($\Delta = 0.1$)
2.00	2.0609 ± 0.0140	-2.5861 ± 0.0037
1.70	1.6444 ± 0.0041	-1.5969 ± 0.0056
1.41	1.2156 ± 0.0023	-0.0293 ± 0.0040
1.35	1.1891 ± 0.0109	0.1000 ± 0.0053
1.27	1.1433 ± 0.0013	0.2145 ± 0.0061
1.20	1.0093 ± 0.0053	0.3201 ± 0.0056

Chapter 5

Conclusions and Outlook

We have shown that the bridge function constructed based on the OZ3 theory can improve over traditional closures, such as the Percus-Yevick (PY) or the hypernetted chain (HNC) equations. The CA-OZ3 formulation can reproduce the depletion behaviour in the Yukawa fluids near an hard wall. Comparisons were made with the predictions of other density functional theories reported in the literature: the fundamental measure theory (FMT) and the inhomogeneous integral equation of Lovett-Mou-Buff-Wertheim. The CA-OZ3 compares favourably to these alternatives when checked against MC data. We achieved quantitative agreement, in general, for wall distances $z > 2$. For $z < 2$ we found some discrepancies in the curvatures of the density profiles. We identified the source of the problem in the short separation values of the adopted bridge functions. Clearly, improvement is needed. By using the approach based on the triplet correlation functions as reported in Ref. [94], we believe that we can develop a better approximation to the triplet total correlation function $h^{(3)}$ than the simple convolution approximation of Jackson and Feenberg. This will be investigated in the future.

In order to solve the Euler-Lagrange equation, the uniform-fluid pair direct correlation function $C_0^{(2)}$ is needed as an input function. Its accuracy critically affects the adsorption profile ($y_w(z)$). This fact has been known, but has not been well documented. In most studies, some mention was made of the construction of $C_0^{(2)}$ but no details were given. No rigorous testing was reported. In our thesis, we considered the effect of three different choices for the uniform Yukawa fluid $C_0^{(2)}$, namely the modified HNC (MHNC), PY, and zero-separation (ZSEP) theories. Their effect on the density profile $y_w(z)$ was clearly shown and results ranked according to their reliability. We also examined the functional dependence of the bridge function B_w on the indirect correlation function γ_w. The Duh-Haymet plot was constructed and allowed us to conclude that the renormalized γ_H gives a better, smoother fit for the B_w as a function, regardless of the specific form of the theory adopted for the homogeneous fluid.

When studying the hard-core Yukawa (HCY) mixture with Monte Carlo computer simulations we were able to show the problem in the simulation results already published in the scientific

literature, which turned out to be affected by severe finite-size effects. Our study was particularly beneficial to those statistical-mechanical theories which have already been assessed against those results, including mean spherical approximation (MSA) [9, 87], analytic equations of state [113], and approaches based on the Ornstein Zernike equation in the MSA approximation [114], where an accumulative parameter is adopted to express thermodynamic quantities. The production of reliable MC data for the HCY mixtures is the first step in the assessment of the extension of our theoretical approach to inhomogeneous, binary mixtures of fluids.

Chapter 6

Bibliography

[1] C. Caccamo, Phys. Rep. **274**, (1996).

[2] E. Waisman, Mol. Phys. **25**, 45 (1973).

[3] J. S. Hϕye and G. Stell, Mol. Phys. **32**, 195 (1976); **32**, 209 (1976).

[4] J. S. Hϕye and G. Stell, J. Chem. Phys. **67**, 439 (1977).

[5] J. S. Hϕye and G. Stell, Mol. Phys. **52**, 1071 (1984).

[6] D. Duh and L. Mier-Y-Teran, Mol. Phys. **90**, 373 (1997).

[7] D. Henderson, E. Waisman, J.L. Lebowitz, and L. Blum, Mol. Phys. **35**, 241 (1978).

[8] J. Konior and C. Jedrzejek, Mol. Phys. **55**, 187 (1985); J. Konior, *ibid.* **68**, 129 (1989).

[9] C. Rey, L. J. Gallego, and L. E. Gonzalez, J. Chem. Phys. **96**, 6984 (1992).

[10] E. Lomba and N.E. Almarza, J. Chem. Phys. **100**, 8367 (1994).

[11] M. H. J. Hagen and D. Frenkel, J. Chem. Phys. **101**, 4093 (1994).

[12] L. Mederos and G. Navascues, J. Chem. Phys. **101**, 9841 (1994).

[13] C. Caccamo, G. Giunta, and G. Malescio, Mol. Phys. **84**, 125 (1995).

[14] D. Pini, G. Stell, and N.B. Wilding, Mol. Phys. **95** 483 (1998).

[15] P. Bolhuis, M. Hagen, and D. Frenkel Phys. Rev. E **50**, 4880 (1994).

[16] A. P. Gast, C. K. Hall, and W. B. Russel, J. colloid Interface Sci. **96**, 251 (1983).

[17] S. Karanikas, J. Dzubiella, A. Moncho-Jorda, and A.A. Louis, J. Chem. Phys. **128**, 204704 (2008)

[18] M. H. J. Hagen and D. Frenkel, FOM Institute for Atomic and Mol. Phys. **101** 4093 (1994).

[19] C. Caccamo, G. Pellicane, and D. Costa, J. Phys. Condens. Matter **12** A437 (1999)

[20] G. Pellicane, D. Costa, and C. Caccamo, J. Phys. Condens. Matter **16** S4923 (2004)

[21] C. Caccamo and G. Pellicane, J. Chem. Phys. **117** 5072 (2002).

[22] Rosenbaum, D. F.; Zamora, P. C.; Zukoski, C. F. Phys. ReV. Lett. **1996**, 76, 150.

[23] Malfois, M.; Bonnete, F.; Belloni, L.; Tardieu, A. J. Chem. Phys. **1996**, 105, 3290.

[24] George A and Wilson W 1994 *Acta Crystallogr.* D **50** 361.

[25] Muschol M and Rosenberger F 1997 J. Chem. Phys. **107** 1953

[26] ten Wolde P R and Frenkel D 1997 **Science 277** 1975

[27] Haas C and Drenth J 2000 *J. Phys. Chem.* **104** 368

[28] E.N. Rudisill and P.T. Cummings, Mol. Phys. **68**, 629 1990; Y.V. Kalyuzhnyi and P.T. Cummings, *ibid.* **87**, 1459 1996.

[29] Y. Yu, and F. You, J. Chem. Phys. **110**, 334 (2006).

[30] *Structure and Dynamics of Strongly Interacting Colloids and Supramolecular Aggregates in Solution*, Nato Asi Series C Kluwer Academic, Dordrecht, 1992, Vol. 369.

[31] G. Pellicane, D. Costa, and C. Caccamo, J. Phys. **108**, 7538 (2004)

[32] URL = ¡http://www.medicalnewstoday.com/articles/153188.php

[33] P. Attard, Adv. Chem. Phys. **92**, 1 (1996).

[34] I. Prigogine, and S. A. Rice, *Advances in chemical physics*, **92** (1996).

[35] van der Waals, J. D.; Kohnstamm, P. *Lehrbuch der Thermodynamik;* Mass & van Suchtelen: Leipzig, 1908; Vol. 1.

[36] Cahn, J. W.; Hillard, J. E. Free Energy of a Nonuniform System. I. Interfacial Free Energy. *J. Chem. Phys.* **1958**, *28*, 258.

[37] See, e.g., Curtin, W. A.; Ashcroft, N. W. Weighted-density-functional theory of inhomogeneous liquids and the freezing transition. *Phys. ReV. A* ***1985, 32, 2909.*** Density-functional theory and freezing of simple liquids. *Phys. ReV. Lett.* ***1986, 56, 2775.***

[38] Denton, A. R.; Ashcroft, N. W. Modified weighted-density-functional theory of nonuniform classical liquids. *Phys. ReV. A* **1989**, *39*, 4701. Reply to Comment on Modified weighted-density-functional theory of nonuniform classical liquids . *Phys. ReV. A* **1990**, *41*, 2224. Weighted-density-functional theory of nonuniform fluid mixtures: Application to freezing of binary hard-sphere mixtures. *Phys. ReV. A* **1990**, *42*, 7312.

[39] Lovett, R.; Mou, C. Y.; Buff, F. P. *J. Chem. Phys.* **1976**, *65*, 2377. Wertheim, M. S. Correlations in the liquid-vapor interface. *J. Chem. Phys.* **1976**, *65*, 2377. Zwanzig, R.; Triezenberg, D. G. Fluctuation Theory of Surface Tension. *Phys. ReV. Lett.* **1972**, *28*, 1183.

[40] Denton, A. R.; Ashcroft, N. W. Density-functional approach to the structure of classical uniform fluids. *Phys. ReV. A* **1991**, *44*, 1219.

[41] S. Q. Zhou and E. Ruckenstein, J. Chem. Phys. **112**, 8079 (2000).

[42] S. C. Kim and S. H. Suh, J. Chem. Phys **117**, 9880 (2002).

[43] S.-C. Kim, B.-S. Seong, and S.-H. Suh, J. Chem. Phys. **131**, 134701 (2009).

[44] M. Lu, M. A. Bevan, and D. M. Ford, J. Chem. Phys. **127**, 164709 (2007).

[45] J. W. Perram and L. R. White, Faraday Discuss. **59**, 29 (1975).

[46] D. Henderson, F. F. Abraham, and J. A. Barker, Mol. Phys. **31**, 1291 (1976).

[47] M. Oettel, J. Phys.: Condens. Matter **17**, 429 (2005).

[48] D. E. Sullivan, D. Levesque, and J.-J. Weis, J. Chem. Phys. **72**, 1170 (1980).

[49] W. Olivaves-Rivas, L. Degrve, D. Henderson, and J. Quintana, J. Chem. Phys **106**, 8160 (1997).

[50] R. Evans, P. Tarazona, and U. M. Berttolo-Marconi, Mol. Phys. **50**, 993 (1983).

[51] L. L. Lee, J. Chem. Phys. **135**, 204706 (2011).

[52] J. K. Singh, Molecular Simulation, **35**, 880 (2009).

[53] C. Jedrzejek and G. A. Mansoori, Acta Physica Polonica **A57**, 107 (1980).

[54] D. J. Gonzalez and M. Silbert, J. Phys. C: Solid State Phys. **16**, L1097 (1983).

[55] J. Konior and C. Jedrzejek, Mol. Phys. **63**, 655 (1988).

[56] J .Krejci, I. Nezbeda, R. Melnyk, and A. Trokhymchuk J. Chem. Phys. **133**, 094503 (2010)

[57] J. M. Kim, R. Castaneda-Priego, Y. Liu, and N. J. Wagner, J. Chem. Phys. **134**, 064904 (2011).

[58] S. Hslushak, J. Chem. Phys. **143**, 124906 (2015).

[59] Y. Rosenfeld, J. Chem. Phys. **98**, 8126 (1993).

[60] Y.-Z. Lin, Y.-G. Li and J.-D. Li, J. Mol. Liquids **125**, 29 (2006).

[61] J. S. Rowlinson, Physica A **156**, 15 (1989).

54

[62] S.-H. Chen, M. Broccio, Y. Liu, E. Fratinid and P. Baglioni, J. Appl. Cryst. **40**, s321 (2007).

[63] M. Bahaa Khedr, Int. J. Mod. Phys. B **20**, 3373 (2006).

[64] S. M. Osman, I. Ali, and R. N. Singh, Phys. Rev. E **87**, 012122 (2013).

[65] M. Dijkstra, Phys. Rev. E **66**, 021402 (2002).

[66] M. Gonzalez-Melchor, A. Trokhymchuk, and J. Alejandre, J. Chem. Phys. **115**, 3862 (2001).

[67] K. P. Shukla, J. Chem. Phys. **112**, 10358 (2000).

[68] G. Rickayzen, and A. Augousti, Mol. Phys. **52**, 1355 (1984).

[69] G. Rickayzen, P. Kalpaxis, and E. Chacon, J. Chem. Phys. **101**, 7963 (1994).

[70] P. Tarazona, Phys. ReV. A **31**, 2672 (1985).

[71] P. Tarazona, U. M. Bettolo Marconi, and R. Evans, Mol. Phys. **60**, 573 (1987).

[72] J. -H. Yi, and S. -C. Kim, J. Chem. Phys. **107**, 8147 (1997).

[73] F.Q. You, Y.X. Yu, and G.H. Gao, J. Phys. Chem. B **109**, 3512 (2005)

[74] A. Trokhymchuk, D. Henderson, and S. Sokolowski, Mol. Phys. **86**, 1339 (1995).

[75] P. T. Cummings and E. R. Smith, Mol. Phys. **38**, 997 (1979); Chem. phys. **42**, 241 (1979).

[76] P. T. Cummings and G. Stell, J. Chem. Phys. **78**, 1978 (1983).

[77] D. Henderson, E. Waisman, J. L. Lebowitz and L. Blum, **35**, 241 (1978).

[78] G. A. Mansoori and N. Kioussis, J. Chem. Phys. **82**, 2076 (1985).

[79] A. Kloczwoski, and A. Samborski, J. Chem Phys. **88**, 5834 (1988).

[80] M. Renkin, and J. Hafner, J. Chem. Phys. **94**, 541 (1991).

[81] B. Smit, and D. Frenkel, Mol. Phys. **74**, 35 (1991); J. Chem. Phys. **94**, 5663 (1991).

[82] C.N. Patra and G.D. Smith, J. Chem. Phys. **124**, 016101 (2006)

[83] D. Pini, M. Tau, A. Parola, and L. Reatto, Phys. Rev. E **67**, 046116 (2003).

[84] A. Parola and L. Reatto, Adv. Phys. **44**, 211 (1995); A. Reiner and G. Kahl, Phys. Rev. E **65**, 046701 (2002); J. Chem. Phys. **117**, 4925 (2002).

[85] E. Scholl-Paschinger, D. Levesque, J. -J. Weis, and G. Kahl, J. Chem. Phys. **122**, 024507 (2005).

[86] Z. Yang, X. Yang, and Z. Xu, Journal of Membrane Science, **320**, 381 (2008).

[87] C. Rey, L. E. Gonzalez, L. J. Gallego, and D. J. Gonzalez, J. Chem. Phys. **100**, 560 (1994).

[88] K. Percus and George J. Yevick, Phys. Rev. **110**, 1 (1958).

[89] M. Lozada-Cassou r. Saavedra-Barrera and d Henderson, J. Chem. Phys. **77**, 5150, (1982).

[90] L. S. Ornstein, and F. Zernike, Proc. Acad. Sci. Amst. **17**, 793 (1914).

[91] J.L. Lebowitz and J.K. Percus, J. Math. Phys. **4**, 116 (1963)

[92] L.L. Lee, J. Chem. Phys. **60**, 1197 (1974)

[93] H.W. Jackson and E. Feenberg, Ann. Phys. **15**, 266 (1961)

[94] L.L. Lee, J. Chem. Phys. **139**, 154301 (2013).

[95] R. Evans, Adv. Phys. **28**, 143 (1979)

[96] R. Evans, J. Phys. **2**, 8989 (1990)

[97] R. Evans, J. Phys. **9**, 2375 (1997)

[98] G. Kahl, B. Bildstein, and Y. Rosenfeld, Phys. Rev. E **54**, 5391 (1996)

[99] J. M. Rogers and J.D. Weeks, J. Phys. **20**, 494206 (2008)

[100] H. Iyetomi, Prog. Theor. Phys. **71**, 427 (1984)

[101] I. Brovchenko and A. Oleinikova, in *Handbook of Theoretical and Computational Nanotechnology*, edited by M. Rieth, W. Schommers (American Scientific Publisher, Los Angeles, CA, 2005). Chap. 62.

[102] D. Bonn and D. Ross, Rep. Prog. Phys. **64**, 1085 (2001)

[103] Y. Rosenfeld, Phys. Rev. Lett. **63**, 980 (1989)

[104] Y. Tang, J. Chem. Phys. **121**, 10605 (2004)

[105] E.-Y. Kim, S.-C. Kim, and B.-S. Seong, Fluid Phase Equilib. **308**, 90 (2011)

[106] C. Caccamo, G. Pellicane, and E. Enciso, Phys. Rev. E. **56**, 6954 (1997)

[107] L.L. Lee, D. Ghinasgi, and E. Lomba, J. Chem. Phys. **104** 8058 (1996)

[108] L.L. Lee, J. Chem. Phys. **107**, 7360 (1997)

[109] D.-M. Duh and A.D.J. Haymet, J. Chem. Phys. **97**, 7716 (1992)

[110] Winsberg, Eric, "Computer Simulations in Science", The Stanford Encyclopedia of Philosophy (Summer 2015 Edition), Edward N. Zalta (ed.), URL = ¡http://plato.stanford.edu/archives/sum2015/entries/simulations-science/¿.

[111] D. Frenkel and B. Smit, *Understanding Molecular Simulation*, (Accademic, San Diego, 2001).

[112] C. Hoheisel and R. Zhang, Phys. Rev. A **43**, 5332 (1991).

[113] J. X. Sun Phys. Rev. E **68**, 061503 (2003).

[114] O. Vazquez, J. N. Herrera, L. Blum, Physica A, **325**, 319 (2003).

Appendix 1: The virial equation for a binary mixture

The quantity known as virial W of the forces for a binary mixture has the following expression:

$$W = \sum_{i=j}^{N_A} \mathbf{r}_i \cdot \nabla_i V_N(\mathbf{r}^N) + \sum_{i=j}^{N_B} \mathbf{r}_i \cdot \nabla_i V_N(\mathbf{r}^N), \qquad (6.1)$$

where

$$V_N(\mathbf{r}^N) = \sum_{i>j} v_{ij}^{AA}(\mathbf{r}_{ij}) + \sum_{i>j} v_{ij}^{BB}(\mathbf{r}_{ij}) + \sum_{i \geqslant j} v_{ij}^{AB}(\mathbf{r}_{ij}) \qquad (6.2)$$

is the total energy potential function of the system, that is written as a sum of pairwise-additive potentials.

Now we note that

$$\begin{aligned}
\sum_{i=1}^{N_A} \mathbf{r}_i^A f_i + \sum_{i=1}^{N_B} \mathbf{r}_i^B f_i &= \sum_{i=1}^{N_A} \mathbf{r}_i^A [\sum_{j \neq i}^{N_A} f_{ij}^A + \sum_j^{N_B} f_{ij}^B] + \sum_{i=1}^{N_B} \mathbf{r}_i^B [\sum_{j \neq i}^{N_B} f_{ij}^B + \sum_j^{N_A} f_{ij}^A] \\
&= \sum_{i=1}^{N_A} \sum_{j>i}^{N_A} \mathbf{r}_{ij} f_{ij}^A + \sum_{i=1}^{N_B} \sum_{j>i}^{N_B} \mathbf{r}_{ij} f_{ij}^B + \sum_{i=1}^{N_A} \mathbf{r}_i^A \sum_j^{N_B} f_{ij}^B + \sum_{i=1}^{N_B} \mathbf{r}_i^B \sum_j^{N_A} f_{ij}^A.
\end{aligned} \qquad (6.3)$$

If we elaborate the last two mixed terms separately, we get

$$\begin{aligned}
\sum_{i=1}^{N_A} \mathbf{r}_i^A \sum_j^{N_B} f_{ij}^B + \sum_{i=1}^{N_B} \mathbf{r}_i^B \sum_j^{N_A} f_{ij}^A &= \sum_{i=1}^{N_A} \sum_j^{N_B} \mathbf{r}_i^A f_{ij} + \sum_{i=1}^{N_B} \sum_j^{N_A} \mathbf{r}_i^B f_{ij} \\
&= \sum_{i=1}^{N_A} \sum_j^{N_B} \mathbf{r}_i^A f_{ij} + \sum_j^{N_A} \sum_{i=1}^{N_B} \mathbf{r}_i^B f_{ij} \\
&= \sum_{i=1}^{N_A} [\sum_j^{N_B} \mathbf{r}_i^A f_{ij} + \sum_j^{N_B} \mathbf{r}_j^B f_{ji}].
\end{aligned} \qquad (6.4)$$

By applying Newton's third law to equation (6.4) we get

$$\sum_{i=1}^{N_A}[\sum_{j}^{N_B}\mathbf{r}_i^A f_{ij} + \sum_{j}^{N_B}\mathbf{r}_j^B f_{ji}] = \sum_{i=1}^{N_A}[\sum_{j}^{N_B}\mathbf{r}_i^A f_{ij} - \sum_{j}^{N_B}\mathbf{r}_j^B f_{ij}]$$

$$= \sum_{i=1}^{N_A}\sum_{j}^{N_B} f_{ij}(\mathbf{r}_i^A - \mathbf{r}_j^B) \qquad (6.5)$$

$$= \sum_{i=1}^{N_A}\sum_{j}^{N_B} f_{ij}\mathbf{r}_{ij}^{AB},$$

then the expression (6.3) can be written as

$$\sum_{i=1}^{N_A}\mathbf{r}_i^A f_i + \sum_{i=1}^{N_B}\mathbf{r}_i^B f_i = \sum_{i=1}^{N_A}\sum_{j>i}^{N_A}\mathbf{r}_{ij}f_{ij}^A + \sum_{i=1}^{N_B}\sum_{j>i}^{N_B}\mathbf{r}_{ij}f_{ij}^B + \sum_{i=1}^{N_A}\sum_{j=1}^{N_B}\mathbf{r}_{ij}f_{ij} \qquad (6.6)$$

Finally, the virial equation (6.1) can be written as

$$W(\mathbf{r}) = -\frac{1}{3}[\sum_{i=1}^{N_A}\sum_{j>i}^{N_A}\mathbf{r}_{ij}\nabla_{ij}v(r_{ij}) + \sum_{i=1}^{N_B}\sum_{j>i}^{N_B}\mathbf{r}_{ij}\nabla_{ij}v(r_{ij}) + \sum_{i=1}^{N_A}\sum_{j>i}^{N_B}\mathbf{r}_{ij}\nabla_{ij}v(r_{ij})]$$

$$= -\frac{1}{3}[\sum_{i=1}^{N_A}\sum_{j>i}^{N_A} w(r_{ij}) + \sum_{i=1}^{N_B}\sum_{j>i}^{N_B} w(r_{ij}) + \sum_{i=1}^{N_A}\sum_{j>i}^{N_B} w(r_{ij})] \qquad (6.7)$$

where $w(r_{ij}) = r_{ij}\frac{dv_{ij}}{dr_{ij}}$

If we average out the virial of the forces, it is then easy to show that it is linked to the thermodynamic pressure of the system by the following identity:

$$PV = Nk_BT+ <W> . \qquad (6.8)$$

Obviously, the thermodynamic average of the hard-sphere part of the pair potentials for the HCYM is expressed again in terms of the contact values of the radial distribution functions, as for Eq. 4.19.